Rank aggregation to predict the fundamental frequency of historic masonry towers

Bulletin of Earthquake Engineering
https://doi.org/10.1007/s10518-026-02369-0

ORIGINAL ARTICLE

Rank aggregation to predict the fundamental frequency of historic masonry towers

Alessio Crocetti[1,2] · **Gaetano Miraglia**[1,2] · **Rosario Ceravolo**[1,2]

Received: 27 June 2025 / Accepted: 14 January 2026

Abstract
The fundamental frequency is a key dynamic parameter for evaluating the seismic vulnerability and structural integrity of historic masonry towers. Its estimation with empirical laws is feasible but it is often complicated by the variability in geometric features, material properties, and boundary conditions. This work proposes an original methodology that combines multiple predictive empirical models and laws using a rank aggregation approach based on the Plackett-Luce model. Rather than selecting a single law, the method considers results from empirical equations and data-driven models to produce a unified and more reliable prediction. Two distinct estimation scenarios are examined: one relying exclusively on geometric properties, and another that also takes into account mechanical features. Both are trained and validated on a broad dataset of historic masonry towers. The novelty of the approach lies in its ability to integrate different sources of knowledge while reducing individual model errors. Since many structural characteristics of the towers may be unknown, this method seeks to combine models with different input features, ranging from complex models to simpler formulations based on easily measurable parameters. By exploiting the best features of each candidate and by ranking their contributions, the method shows improved performance across different towers. This strategy can be a valuable tool in structural health monitoring and seismic assessment of heritage towers, especially when experimental dynamic data are not available and when dealing with complex modeling uncertainties.

Keywords Ensemble methods · Fundamental frequency · Historic towers · Plackett-Luce · Rank aggregation · Structural health monitoring

✉ Alessio Crocetti
alessio.crocetti@polito.it

[1] Politecnico di Torino, Corso Duca degli Abruzzi 24, 10129 Turin, Italy

[2] Responsible Risk Resilience interdepartmental Centre (R3C), Politecnico di Torino, Corso Duca degli Abruzzi 24, 10129 Turin, Italy

Published online: 11 February 2026

1 Introduction

Vibration modes are essential parameters for predicting the dynamic and seismic response of structures, and are also effective indicators of structural integrity. However, historic masonry buildings can pose significant challenges even when it comes to estimating their fundamental frequency, as experimental data often fail to align with prediction laws provided by the literature or codes. This discrepancy is largely due to the complex nature of these buildings: variability in material composition, irregular geometries, uncertain boundary conditions, and limited information on construction techniques all contribute to the difficulty. In addition to these, it is important to also point out irregularities between structural components and uncertainties related to material degradation and quality, and past interventions on the building (Saloustros et al. 2020). In the Structural Health Monitoring (SHM) field (Farrar and Worden 2006), the fundamental frequency offers important information about the monolithic nature of the structure and the degree of connection to the constraints and the ground. For Cultural Heritage (CH) assets, such as bell towers, this parameter becomes even more critical, given their historical significance and often unknown construction history. It can be used as a valuable parameter to identify damage conditions in the structure, assess the effectiveness of previous strengthening interventions, and support conservation strategies (Bartoli et al. 2016; Milani et al. 2012).

While in situ dynamic testing provides reliable and detailed information, its application is often constrained by high costs, the need for expert personnel, and logistical complexities. As a result, the estimation of the fundamental frequency is often based on simplified empirical formulations provided by national codes, which, however, were developed for generic masonry structures and are not specifically tailored to historical towers. To address this gap, recent advancements in the field have led to the development of new empirical and hybrid models based on extensive databases, integrating experimental results and numerical analyses to improve predictive capabilities for CH structures (Bartoli et al. 2017, 2020; Çalik et al. 2020; Diaferio et al. 2018; Lopez et al. 2019; Montabert et al. 2023; Rainieri and Fabbrocino 2011; Shakya et al. 2016; Testa et al. 2024).

Numerous studies in literature have proposed formulations to estimate the fundamental frequency of historic towers. Some studies distinguish between towers that are structurally integrated with adjacent buildings and those that are isolated (Bartoli et al. 2020; Diaferio et al. 2018; Manikandan et al. 2024; Testa et al. 2024). In the more common scenario, where the tower is connected to other structures, such as churches, the dynamic response is affected by these interactions. The presence of such connections alters stiffness distribution and boundary conditions, thereby modifying the vibration characteristics of the tower compared to an isolated configuration. For this reason, taking into account the concept of *effective height* becomes essential when aiming to achieve a reliable estimate for the modal properties of a tower. This geometric parameter plays a key role, especially in cases where the structural system is influenced by adjacent elements. The accuracy of empirical and semi-empirical models largely depends on the nature of the input parameters they require. While some approaches rely solely on geometric data (Diaferio et al. 2018; Montabert et al. 2023; Rainieri and Fabbrocino 2011; Testa et al. 2024), making them straightforward and easy to apply, others integrate mechanical properties to provide a more refined prediction of the fundamental frequency (Bartoli et al. 2020; Montabert et al. 2023; Shakya et al. 2016).

Each empirical law originates from a specific dataset and is shaped by the methodological choices adopted. These include the type of structures analyzed, the simplifications introduced, and the fitting criteria adopted. As a consequence, when several of these laws are applied to the same structure, the results can differ significantly. This variability is not necessarily an indication of inaccuracy, but rather a reflection of the differences in the underlying assumptions and scope of application of each formula.

Instead of selecting a law arbitrarily or relying solely on expert judgment, it is possible to frame the selection process as a ranking problem (Guiver and Snelson 2009; Yasutake et al. 2012). In this framework, each empirical formulation is treated as a candidate that provides an estimate of the fundamental frequency. These estimates are then compared to experimentally measured values, which are used as a reference. Each measurement can be interpreted as a vote, expressing a preference for the laws that produce results closer to the actual observed frequency.

This approach makes it possible to objectively evaluate multiple empirical formulations at the same time. By aggregating the preferences expressed by different experimental observations, it is possible to identify the formulation that performs best across a wide range of cases. The goal of this procedure is to reduce subjectivity in the selection process and to establish a reliable method for ranking the available empirical laws, especially when dealing with large datasets and variable structural configurations.

To implement this comparison process in a structured way, a specific methodology based on rank aggregation is adopted. This strategy allows the integration of multiple independent evaluations into a single ranking list that reflects the overall performance of each empirical formulation. In this context, the empirical laws are interpreted as competing candidates, and the experimentally measured frequencies act as independent evaluators. Each evaluator compares the predicted value obtained from every law to the corresponding observed frequency and expresses a score that quantifies the level of agreement. When these evaluations are collected across several structures, it becomes possible to build a set of preferences that relate each candidate law to its prediction accuracy in different conditions.

Through the rank aggregation process, these results are synthesized into a single ranking, which represents the most probable order of reliability among the available empirical laws. The goal is to identify the formulation that tends to produce results closer to the experimental evidence in the majority of cases. This method allows for the selection of a law not only based on its performance in a specific case, but also on its general capacity to provide accurate estimates across a broad and heterogeneous dataset. In this way, the procedure increases the robustness of the frequency prediction and supports the identification of the most appropriate formula for application to historic masonry towers with varying geometric and structural characteristics.

The paper is organized as follows: Section 2 presents the rank aggregation strategy and, more in detail, the Plackett-Luce model, with a focus on an application to the estimation of the fundamental frequency in historic bounded masonry towers. Section 3 highlights the results and a critical discussion is reported, underlining the strengths and limitations of the proposed method. In Sect 4 the conclusions of the study are drawn.

2 Materials and methods

This Section addresses the estimation of the fundamental frequency of historic towers by integrating multiple predictive approaches, including empirical laws available in the literature and in national codes, neural network and Statistical Bayesian Learning (SBL) models (Fuentes et al. 2019). A RA strategy based on the Plackett-Luce model is employed to combine these different estimations, aiming to reduce individual model bias and improve overall robustness. Two scenarios are considered in the analysis: one relying only on geometric parameters (A), and another including both geometric and mechanical properties (B). This dual perspective allows for an evaluation of how different levels of input information affect the accuracy and consistency of the predicted fundamental frequencies. The datasets used for the analyses were constructed and revised starting from an existing dataset (Testa et al. 2023), enriched with additional data and updated geometric and mechanical information.

Section 2.1 presents the empirical laws used for the estimation of the fundamental frequency of historic masonry towers. Section 2.2 introduces the rank aggregation framework based on the Plackett–Luce model adopted for combining the individual predictors. Sections 2.3 and 2.4 describe the implementation of the proposed approach for cases relying only on geometric parameters (A) and on both geometric and mechanical parameters (B), respectively.

2.1 Empirical laws for the estimation of the fundamental frequency of historic masonry towers

2.1.1 Empirical laws based on geometric parameters for masonry towers

Empirical formulations based on geometric parameters are commonly used to estimate the fundamental frequency when dynamic testing is not available. Among the most widely adopted are those included in national codes, such as NTC 2018 (Italian Technical Standards for Construction) and NCSE-02 (Norma de Construcción Sismorresistente). These codes offer simplified laws derived from limited datasets, primarily focused on low-rise, conventional masonry buildings. The first includes only the total height H as independent variable for the fundamental frequency estimation of masonry structures:

$$f_1 = \left(0.050 H^{3/4}\right)^{-1}, \tag{1}$$

while the NCSE-02 considers both H and L, with L being the plan dimension of the building in the direction of oscillation:

$$f_1 = \frac{\sqrt{L}}{0.06\sqrt{\frac{H}{2L+H}}}. \tag{2}$$

These equations are convenient and accessible, but they do not take into account the specificity represented by historic bell towers. These often present unique dynamic behavior influenced by vertical irregularities, varying material quality, and the interaction with adjacent structures (e.g., churches), especially in the case of bounded towers. Recognizing this,

recent research has moved towards more specialized formulations. In addition, the Italian guideline DPCM (2011) (Decreto del Presidente del Consiglio dei Ministri, 9 febbraio 2011) introduced a linear formulation (Faccio et al. 2010) which establishes a direct relation between the fundamental frequency and the total height H of the tower for heritage structures. The equation was calibrated on a set of historic slender towers, and it is particularly effective for predicting fundamental frequencies over 1 Hz, which are typical of many bell towers and minarets.

A significant advancement over standard code formulations was proposed by Rainieri and Fabbrocino (2011), leading to an improved correlation for masonry towers based on a dataset of 30 Italian towers.

Subsequent works have highlighted the importance of expanding the parameter set beyond height only based metrics. For instance, Shakya et al. (2016) considered a dataset of 59 masonry towers and proposed, in particular, different geometric-only formulations based on H and the lowest plane width dimension at base $L_{\min}$. Other formulations were proposed to differentiate between typological groups of structures, such as minarets, industrial chimneys, and bell towers (Bayraktar et al. 2022; Oliveira et al. 2023; Serhatoğlu and Livaoğlu 2019; Shakya et al. 2016). Another important subdivision has been highlighted in the literature between models tailored for predicting the fundamental frequency of isolated vs. bounded towers (Bartoli et al. 2017; Diaferio et al. 2018). It is fundamental to take into account the structural behavior induced by lateral restraint conditions such as surrounding buildings. In this context, the notion of effective height H_{eff} was introduced. To better explain, H_{eff} is defined as the portion of the tower that vibrates freely. The inclusion of this parameter allowed for more accurate representations of boundary conditions without relying on mechanical properties. Bartoli et al. (2017) showed that prediction accuracy improves when using H_{eff} rather than H, and when accounting for the base side length of the tower L as an additional geometric parameter.

In this context, Diaferio et al. (2018) proposed distinct empirical formulations for 6 isolated and 18 bounded towers, minimizing estimation error through exponential regression models. For bounded towers, their models exploit different geometric properties, such as H, H_{eff}, and $L_{\min}$. Similarly, Montabert et al. (2023) developed empirical models based on a large dataset, presenting an interaction factor based on the ratio between the interaction height ($H-H_{eff}$) and H. In one of the most extensive recent contributions, Testa et al. (2024) introduced regression models based on a large dataset of 184 historic masonry towers, accounting for multiple geometric features, such as H, H_{eff}, $L_{\min}$, $L_{\max}$, and the wall thickness s. In as many as 72 of the case studies, some geometric characteristics were unknown. In this work, the height (i.e., total and effective) is confirmed to be the dominant predictor of the first natural frequency of historic masonry towers, exhibiting a clear non-linear inverse relationship in which frequency increases rapidly as height decreases (Testa et al. 2024).

Finally, it is worth noting that some of the larger datasets actually incorporate smaller datasets present in already published studies; therefore, the datasets are not entirely independent but rather differ in terms of completeness and level of detail (e.g., geometric properties involved).

2.1.2 Empirical laws based on both geometric and mechanical parameters for masonry bell towers

Slender towers are commonly idealized as cantilever structures due to their main vertical configuration and base restraints. This assumption allows an initial approximation of their dynamic behavior (e.g., fundamental natural frequency) using the beam theory. In detail, when modelled as slender cantilevers with hollow square sections, their fundamental frequency f_1 can be expressed through classical analytical formulations:

$$f_1 = \frac{1.875^2}{2\pi H_{eff}^2}\sqrt{\frac{EJ}{\rho A}}, \tag{3}$$

where E is the Young's modulus, J is the moment of inertia, ρ is the material density and A is the cross-sectional area.

However, real-world towers often diverge from this equation. The H_{eff} is used to mitigate one of the issues regarding the presence of adjacent buildings that partially constrain the lateral displacement of the tower. Irregularities in the geometry are always present, such as cross-sectional variation along the height of the structure, often due to the presence of large or irregularly distributed openings. Bartoli et al. (2020) investigated the influence of façade openings on the fundamental frequency of historic masonry towers by combining experimental data from a database which includes 11 isolated and 45 confined towers with an extensive set of parametric analyses based on numerical modeling. It is also assumed that the material is homogeneous, i.e. a unique E and ρ for all the main body of the tower. This does not reflect the actual configuration, for instance, of historic bell towers, which often present heterogeneous materials along their height due to construction in different historical periods, seismic interventions and reconstructions, or local strengthening following damage from various events that occurred during their lifespan (Oliveira et al. 2012; Ramos et al. 2010; Scussolini et al. 2023). These factors significantly influence the dynamic response, making a direct application of classical theory insufficient for accurate frequency prediction.

Shakya et al. (2016) proposed different variations of Eq. (3), by taking into account the total height H and a coefficient X that pre-multiplies EJ for different masonry buildings, such as all types of masonry slender structures (X= 1.425), or, more specifically, masonry tower structures (X= 1.375), and masonry minaret structures (X= 1.345).

Bartoli et al. (2017) proposed different formulations by accounting for the velocity of propagation of the elastic compression waves (P-waves) through masonry:

$$v_p = \sqrt{\frac{E}{\rho}\frac{(1-v)}{(1+v)(1-2v)}} \cong \sqrt{\frac{E}{\rho}}, \tag{4}$$

where v is the Poisson's ratio. Approximating the second expression under the square root in the range 1.0–1.1 for typical values of $v \leq 0.25$, one can use the approximated expression. By taking into account Eq. (3), the same authors proposed different formulations as a function of H_{eff} and v_p.

Recently, Montabert et al. (2023) introduced physics-based formulations to evaluate the fundamental frequency of masonry towers. Regression models and Artificial Neural

Network (ANN) have been also exploited, e.g. by Manikandan et al. (2024), to predict fundamental frequency of slender masonry structures, including minarets, starting from geometric and mechanical properties.

2.2 Rank aggregation using the Plackett–Luce model for fundamental frequency estimation of historic bounded masonry towers

When multiple predictive formulas produce comparable outcomes, as is often the case in estimating the fundamental frequency of historic towers, it is important to determine a strategy that provides a general and reliable result. Rather than evaluating each individual formulation, the problem can be framed as one of ordering: each empirical law is treated as a candidate, and the task becomes ranking them according to their predictive agreement with experimental data. This leads naturally to a ranking problem (Yasutake et al. 2012), where a series of partial orderings, each derived from individual frequency measurements, are combined to form a comprehensive hierarchy of performance.

The rank aggregation (RA) problem (Cao et al. 2007; Coletta et al. 2020; Guiver and Snelson 2009; Miraglia et al. 2019; Yasutake et al. 2012) consists of determining the most representative ordering of I candidates. This is done by analyzing multiple ranking lists, each produced by one of the K available voters.

To address this problem effectively, several mathematical models have been proposed, among which the Plackett-Luce (PL) model (Guiver and Snelson 2009; Luce 1959; Plackett 1975) has shown particularly strong capabilities in capturing the ranking information. K corresponds to the number of voters (each associated with a specific experimental observation) and I denotes the number of candidates, for instance the estimation laws for the fundamental frequency.

Regarding the number of candidates I, it is important to note that this value is typically restricted to a range between 2 and 12 (The MathWorks Inc 2022). The minimum value ensures that multiple models can be meaningfully compared, allowing for the benefits of combining diverse estimation strategies. On the other hand, the upper limit is imposed by computational constraints. As the number of candidates increases, the total number of possible ranking permutations grows factorially, reaching $I!$. When I exceeds 12, the number of permutations becomes extremely large, making it impractical to store or process all combinations with standard computing resources. For this reason, keeping $I \leq 12$ ensures that the RA remains feasible in terms of memory and computational time. Accordingly, the selection of candidates (i.e., formulations or models) must explicitly account for this constraint.

The PL distribution originates from the independent contributions of Plackett (1975) and Luce (1959), who developed foundational theories on probabilistic choice and ranking. At the core of this model lies Luce's axiom, which describes how choices are made within a subset of items. According to this principle, the likelihood of selecting one item over another depends uniquely on the relative preference between the two and remains unaffected by the presence or absence of additional items in the set. When applied to a group of items associated with predefined probabilities, the selection process develops by choosing one item at a time, following the specified probability distribution. Repeating this sampling process produces a complete ranking of the items, which can be interpreted as a single observation drawn from a larger probability distribution defined over all possible permutations. Plackett initially introduced the structure of this distribution to represent outcome

probabilities in the context of horse racing. When combined with Luce's axiom, the model can be naturally extended to also handle partial rankings. The PL model can be subdivided into three different phases.

2.2.1 Phase 1: Individual assessment

In this first phase, each law is assessed independently by K voters, i.e. the fundamental frequency measurements in the case in question. The set of I candidates comprises the selected estimation laws for bounded historic towers, considering the case where (i) only geometric measurements are available, and (ii) the information of mechanical properties is present. These candidates provide a different predictive expression for the fundamental frequency of bounded towers. In each of the two subsets of laws, each candidate is independently assessed based on its performance in predicting the experimental observation, representing the starting point for the ranking process. The scores are computed based on the scatter discrepancy vector $\beta_{k,i}$, each row containing the specific output being analyzed (in this case the individual tower). Each vector represents the discrepancy between the estimated vector $\mathbf{z}_{k,i}$ provided by the i-th empirical formulation and the corresponding experimental measurement vector $\mathbf{z}_{k,exp}$, which contains the information for all bell towers, associated with voter k:

$$\beta_{k,i} = \frac{|\mathbf{z}_{k,i} - \mathbf{z}_{k,exp}|}{|\mathbf{z}_{k,exp}|}. \tag{5}$$

Based on these scatter vectors, the scores for each candidate are then defined as:

$$\mathbf{w}_{k,i} = \frac{\mathbf{w}^*_{k,i}}{\sum_{i=1}^{I} \mathbf{w}^*_{k,i}}, \tag{6}$$

assuming:

$$\mathbf{w}^*_{k,i} = e^{-\left(\frac{\beta_{k,i}}{\sigma_k}\right)^2}. \tag{7}$$

In Eq. (7), the form assumed for $\mathbf{w}^*_{k,i}$ transforms the problem from a minimization to a maximization framework by applying a zero-mean Gaussian function. In this context, $\boldsymbol{\sigma}_k$ in Eq. (8) indicates the standard deviation of the k-th scatter distribution, computed with respect to the set of empirical formulations:

$$\boldsymbol{\sigma}_k = \sqrt{\frac{1}{I-1}\sum_{i=1}^{I}\left(\beta_{k,i} - \overline{\beta}_k\right)^2}. \tag{8}$$

To illustrate the application of the RA process, it is possible to adopt the voter-candidate analogy. Considering K voters and I candidates: each voter independently evaluates all candidates and expresses a preference, for instance assigning scores that individuate a ranking. Fundamentally, no voter knows in advance which candidate will be the best. The aim is

therefore to combine multiple evaluations into a collective decision that estimate the best outcome (Fig. 1). Here, the "reference solution" does not coincide with the experimental measurement itself; rather, it refers to the RA of the estimation laws that is inferred by the PL model as the most likely one, given the discrepancy vectors $\beta_{k,i}$ computed with respect to the experimental data $\mathbf{z}_{k,exp}$.

In this analogy, voters correspond to the K scatter discrepancy vectors $\beta_{k,i}$ (Eq. (5)), which are, as above stated, directly linked to the experimental measurements, $\mathbf{z}_{k,exp}$. On the other hand, candidates correspond to the I estimation laws. Each voter gives a score after observing the performance of every candidate. This leads to K individual score-based rankings, one per voter (Fig. 2).

2.2.2 Phase 2: Individual judgement on ranking permutations

In Phase 2, all possible ranking lists of the estimation laws are systematically generated. Considering that there are I estimation laws in total for the specific case (geometric parameters only or geometric-and-mechanical parameters), one can construct a vector of permutation indices, denoted as $\mathbf{t}=[1,2,\ldots,i,\ldots,I]$. The permutation matrix $\mathbf{C}$, which includes all P possible orderings of the candidates, is generated as $\mathbf{C}=\text{perms}(\mathbf{t})$. This matrix has dimensions $P \times R$, where $P=I!$ is the total number of permutations, and $R=I$ corresponds to the number of candidates. Thus, $\mathbf{C} \in \mathbb{N}^{P \times R}$. The voter related to the fundamental frequency must now assess every permutation based on the scores they previously assigned during the individual evaluation stage (Section 2.2.1). After the definition of the permutation matrix $\mathbf{C}$, each voter assesses the likelihood of each possible ordering of the candidates. For every

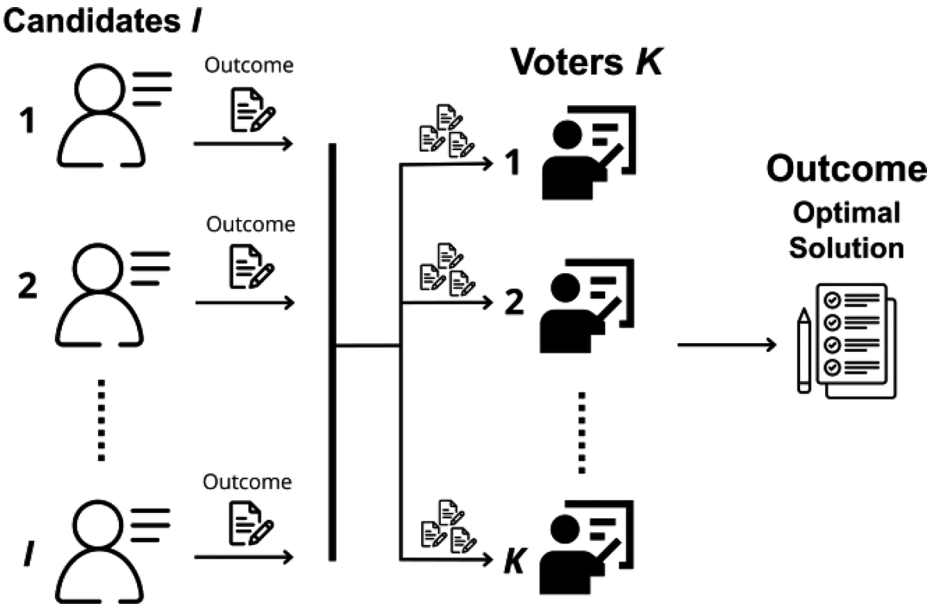

Fig. 1 The *voters* (fundamental frequency obtained through experimental measurements, expressed as discrepancy $\beta_{k,i}$ from estimations) rank the different *candidates* (fundamental frequency estimation laws), to select an optimal outcome through a RA strategy based on the PL model

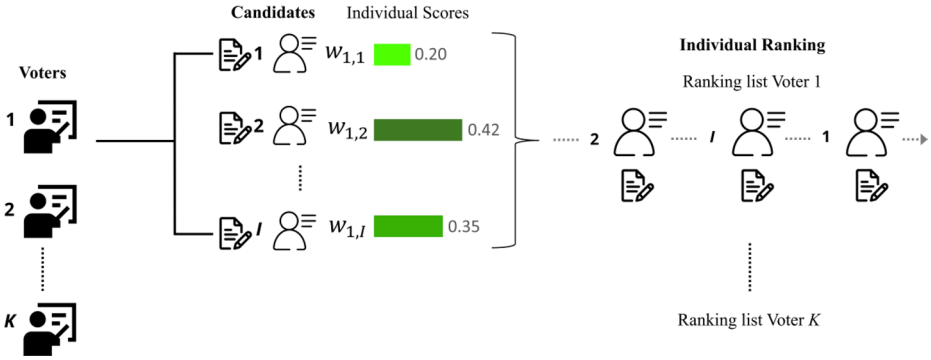

Fig. 2 The *voters* (fundamental frequency obtained through experimental measurements, expressed as discrepancy $\beta_{k,i}$ from estimations) independently assess each different *candidate* (estimation laws) providing a score ($w_{k,i}$) and defining their individual rankings

permutation p and for each voter k, the probability $\mathbf{f}_{p,k}$ of observing a specific ranking is calculated based on the scores attributed in the previous stage as:

$$\mathbf{f}_{p,k} = \prod_{r=1}^{R} \frac{\mathbf{w}_{k,C_{p,r}}}{\sum_{s=r}^{R} \mathbf{w}_{k,C_{p,s}}}, \tag{9}$$

where $\mathbf{w}_{k,C_{p,r}}$ represents the weight assigned by voter k to the candidate located in the r-th position of the p-th permutation, denoted as $C_{p,r}$. The total number of candidates is given by $R=I$, and s is introduced as an auxiliary index used in the computation. Each voter performs this evaluation independently, assigning a probability to every possible permutation.

Following the analogy, this phase corresponds to the *voters* revisiting their initial score-based classification of the *candidates* and analyzing all possible permutations, thereby generating a finite set of ranking lists and a finite number of possible outcomes.

2.2.3 Phase 3: Group assessment and identification of the best ranking

In this final phase, the K *voters* collaborate to determine the most representative ranking list. Once the reference ranking has been identified, the relative positions of all candidates are established, from the best to the worst. The collective assessment is based on the likelihood of each permutation being observed. Since the probabilities $\mathbf{f}_{p,k}$ associated with each permutation p were computed independently by each voter k, the joint likelihood of observing a specific ranking is obtained by multiplying these individual values. This yields the compound probability $\mathbf{f}_p$ (Eq. (9)), which quantifies the overall plausibility of each permutation across all voters:

$$\mathbf{f}_p = \prod_{k=1}^{K} \mathbf{f}_{p,k} = \prod_{k=1}^{K} \left(\prod_{r=1}^{R} \frac{\mathbf{w}_{k,C_{p,r}}}{\sum_{s=r}^{R} \mathbf{w}_{k,C_{p,s}}} \right). \tag{10}$$

The permutation that yields the highest value of Eq. (10), once summed for all the bell towers, corresponds to the most probable ranking to be observed f_{p*} and is therefore selected as the optimal ordering, according to the principle of maximum likelihood. This ranking is denoted by $a^* = C_{p^*,\forall r}$, where p^* is the index of the row in the permutation matrix $\mathbf{C}$ that maximizes Eq. (10).

In the analogy, this corresponds to the moment when all the *voters* compare the scores they assigned to the *candidates*. Although each formed their preference independently, they now agree to combine their perspectives by aggregating the likelihoods assigned to each possible ranking. The result is a shared probability value for each permutation in the matrix $\mathbf{C}$, representing the collective belief about which outcome is the optimal one. As shown in Fig. 3, this step concludes the ranking process by identifying the list that best represents the evaluations of all voters.

2.2.4 Weighting strategies

Once the most likely ranking list has been established, the voters must decide how to extract the final outcome. This can involve selecting the candidate positioned first in the ranking or, alternatively, adopting a strategy that combines the results of multiple candidates, depending on the intended decision criterion.

Different strategies can be adopted to derive a final estimate from the reference list. These weighting strategies define how much influence each candidate (i.e., estimation law) has on the final outcome, depending on its position in the ranking. Some approaches might assign equal weight to the top *n* candidates, effectively averaging their results regardless of their precise order, while others might apply exponential decay, where the influence of each candidate decreases rapidly with its position. Within the alternative approaches, a common method is to consider only the top-ranked candidate, treating it as the sole contributor to the final decision. In the field of information retrieval, such weighting strategies are commonly

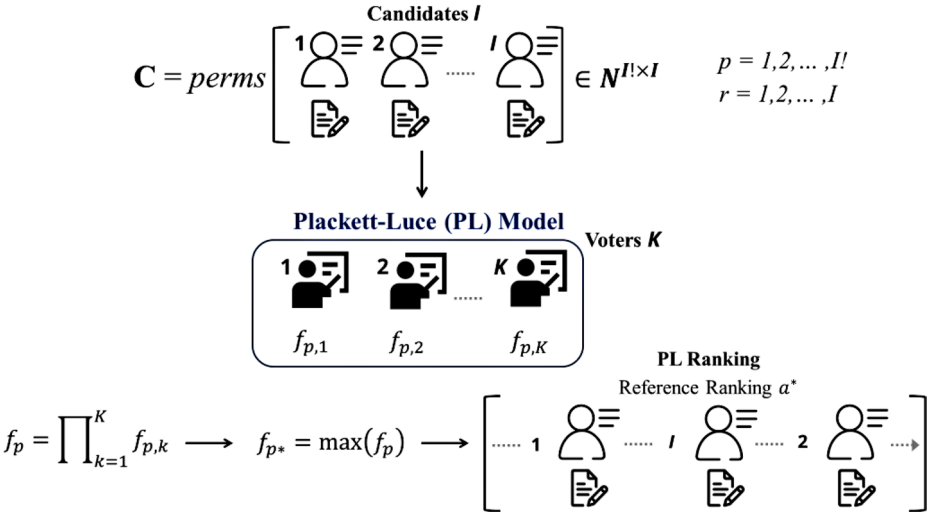

Fig. 3 Following the PL model, *voters* can obtain an optimal outcome by relying on a unique ranking a^* of the *candidates.* From the permutation matrix $\mathbf{C}$, the permutation that yields the highest value of f_p, once summed over all the elements, corresponds to the most probable ranking to be observed, f_{p*}

referred to as *evaluation measures*, and several studies have explored their applicability (Bama et al. 2015).

One possible approach for this combination is the mean reciprocal rank (MRR), which involves computing a weighted average of the candidates outcome (e.g., estimation laws), giving greater importance to those that appear earlier in the selected ranking list (typically, the first three or four). In this scheme, each treatment contributes to the final result in proportion to its rank, with higher-ranked treatments having a larger influence on the aggregated value. In this paper, the MRR outcome vector $\mathbf{z}_{MRR}$ can be defined as:

$$\mathbf{z}_{MRR} = \frac{\sum_{r=1}^{R} \frac{1}{r} \mathbf{z}_{a_r^*}}{\sum_{r=1}^{R} \frac{1}{r}}, \tag{11}$$

where R is the total number of candidates (i.e., estimation laws), r is the position of the candidate in the reference ranking list a^*, and $\mathbf{z}_{a_r^*}$ is the predicted vector (i.e., fundamental frequency for all the bell towers) provided by the candidate ranked at position r. This formulation ensures that higher-ranked predictions have a greater impact on the final result, while still considering the contribution of all candidates.

To compare the results, different weighting techniques have been used in this study:

- MRR:

$$\alpha_r^{MRR} = \frac{1/r}{\sum_{j=1}^{R} \frac{1}{j}}. \tag{12}$$

- Exponential weighting:

$$\alpha_r^{exp} = \frac{e^{-\lambda r}}{\sum_{j=1}^{R} e^{-\lambda j}}, \tag{13}$$

where $\lambda = 1 > 0$ is a decay parameter.

- Linear weighting with threshold:

$$\alpha_r^{thr} = \frac{\max(0, \tau - r)}{\sum_{j=1}^{R} \max(0, \tau - j)}, \tag{14}$$

where $\tau = R - round(0.2R)$ is a threshold parameter, such that the lowest 20% of the ranked laws receive a weight of zero.

- Linear weighting:

$$\alpha_r^{lin} = \frac{\max(0, \tau_{lin} - r)}{\sum_{j=1}^{R} \max(0, \tau_{lin} - j)}, \tag{15}$$

where $\tau_{lin} = R + round\,(0.2R)$ is a parameter that controls the rate of linear decay of the weights.

Figure 4 shows the different weighting techniques for an assumed value of ranking positions equal to 10. Lastly, In Fig. 5, a flowchart of the proposed methodology is reported.

2.3 Estimation of the fundamental frequency for historic bounded masonry towers through geometric-only parameters (A)

In this first analysis, the effectiveness of the proposed RA strategy is assessed using only geometric parameters coming from extensive datasets of geometric parameters related to historic masonry towers. Herein, eight different candidates are considered to estimate the fundamental frequency of these towers: (i) six different empirical laws from literature, (ii) a developed neural network model, and (iii) a SBL model.

In this study, the terms "training" and "validation" set are used consistently across both empirical and data-driven approaches for clarity in the comparison. However, it is important to note that, for the empirical laws, these terms do not imply an actual training or validation process as in data-driven models. In this case, they simply refer to the reference datasets adopted for the development and assessment of the different formulations. On the other hand, for the SBL and neural network models, the same datasets are effectively employed in a training-validation/testing procedure required for implementing the RA strategies.

2.3.1 Fundamental frequency estimation laws (A)

Firstly, six different fundamental frequency estimation laws for masonry towers are exploited. These are selected from literature, ensuring they reflect diverse geometric char-

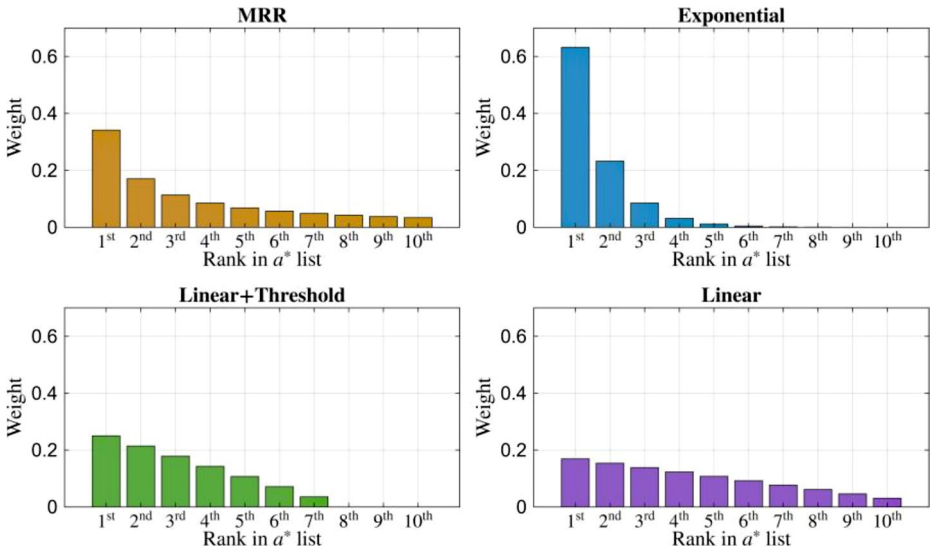

Fig. 4 Proposed weighting strategies for 10 hypothetical candidates. (MRR = mean reciprocal ranking, Exp. = exponential decay, Linear + Thr. = Linear with a threshold, and Linear). Each plot illustrates how the assigned weight varies with the candidate position in the ranking, reflecting its relative influence on the final aggregated results

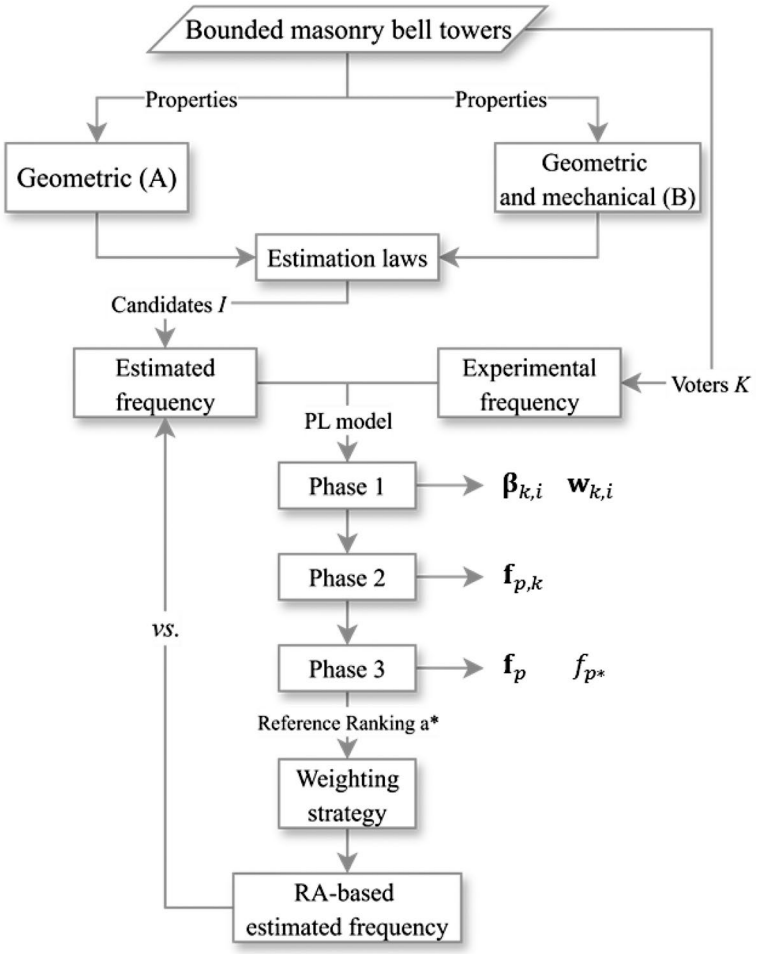

Fig. 5 Flowchart describing the proposed methodological framework

acteristics and derive from varied tower datasets. As detailed in Table 1, the chosen laws differ in complexity and required input parameters.

- Rainieri and Fabbrocino (2011) consider only H;
- Shakya et al. (2016) use L_{min}, H_{eff}, and H;
- Montabert et al. (2023) take into account H and the ratio between H_{eff} and H.
- Testa et al. (2024) selected formulations using only H_{eff} (a), and another also using H_{eff}, L_{min}, L_{max}, and s (b).

This selection guarantees a comprehensive coverage of different combinations of geometric parameters for the frequency estimation of historic bounded towers, also taking into account the computational limitation given by the factorial growth of candidates' permutations corresponding to matrix **C** (Section 2.2).

Table 1 Empirical laws (candidates) for the prediction of the fundamental frequency of towers based on geometric parameters

Reference	Equation (f_1 [Hz])	
Rainieri and Fabbrocino (2011)	$\left(0.0113H^{1.138}\right)^{-1}$	(16)
Shakya et al. (2016)	$\frac{{L_{min}}^{0.17}}{0.03H\left(\frac{H}{L_{min}+H}\right)^{0.5}}$	(17)
Diaferio et al. (2018)	$14.61L_{min}^{-0.254}H_{eff}^{-0.341}H^{-0.216}$	(18)
Montabert et al. (2023)	$23.22H^{-0.695}\left(1-\frac{H-H_{eff}}{H}\right)^{-0.028}$	(19)
Testa et al. (2024) (a)	$11.87H_{eff}^{-0.601}$	(20)
Testa et al. (2024) (b)	$10.43H_{eff}^{-0.75}L_{min}^{0.23}L_{max}^{0.10}s^{-0.06}$	(21)

The table summarizes the six empirical formulations selected from the literature and used as candidate estimation laws in the proposed framework

2.3.2 Sparse Bayesian Learning Model (A)

Sparse Bayesian Learning (SBL) is a Bayesian approach to regression that aims to find a solution by setting to zero the model parameters that do not contribute to explaining the data. The approach is based on identifying a set of potential relationships which describe the observed data through a predefined dictionary of candidate functions. SBL produces a sparse set of weights for a regression model. Contrarily to other regression models, such as Lasso (Ranstam and Cook 2018), SBL operates within a probabilistic framework. The key limitation of classical Lasso requires choosing the degree of sparsity via a penalty term, while SBL works by inferring an appropriate level of sparsity from data through Bayesian evidence maximization. Fuentes et al. (2019) applied this using the Relevance Vector Machine (RVM) (Tipping 2001). Basically, this is a sparse Bayesian regression model that leads to both a set of learned weights and an estimate of prediction uncertainty due to its Bayesian formulation. In this approach, the regression model is written as a linear combination of chosen basis functions:

$$\mathbf{y} = \sum_{i=1}^{N} \mathbf{d}_{\mathrm{i}}\left(\mathbf{x}\right)\gamma_i, \tag{22}$$

with $\mathbf{D}\left(\mathbf{x}\right) = [\mathbf{d}_1, \ldots, \mathbf{d}_{\mathrm{n}}]$representing the basis function set of the input vector $\mathbf{x}$, and $\boldsymbol{\gamma} = [\gamma_1, \ldots, \gamma_n]$ is the weight vector. In this application, the vector $\mathbf{x}$ includes the geometric properties available for each bell tower (H, H_{eff}, L_{min}, L_{max}, and s). The framework enforces sparsity by selecting only the most relevant basis functions from the dictionary $\mathbf{D}\left(\mathbf{x}\right)$ needed to fit the data. The model assumes a source of stochastic noise and model discrepancy, ε, modelled with a Gaussian distribution. The model output is represented by means of the target vector $\mathbf{t}$, such that:

$$\mathbf{t} = \mathbf{y} + \varepsilon. \tag{23}$$

Defining the hyperparameter α, the RVM describes the prior distribution of the parameter vector $p(\boldsymbol{\gamma}|\boldsymbol{\alpha})$. The specific choice of this prior is what enforces sparsity in the model. In detail, a hierarchical Gaussian prior is adopted as:

$$p(\boldsymbol{\gamma}|\boldsymbol{\alpha}) = \prod_{i=1}^{M} \mathcal{N}\left(\gamma_i|0, \alpha_i^{-1}\right). \tag{24}$$

Each element of the hyperparameter vector $\boldsymbol{\alpha} = \{\alpha_1, \ldots, \alpha_n\}$ controls the prior variance of the corresponding weight in $\boldsymbol{\gamma}$. Under the assumption of Gaussian likelihood, the posterior distribution of the parameters is obtained by applying Bayes theorem, which provides the parameters to be used in Eq. (22) at each recursive Bayesian iteration:

$$p\left(\boldsymbol{\gamma}|\mathbf{t}, \sigma^2\right) = \frac{p(\boldsymbol{\gamma}) \cdot p\left(\mathbf{t}, \sigma^2|\boldsymbol{\gamma}\right)}{\zeta}, \tag{25}$$

where σ^2 is the external noise variance and $\zeta = p\left(\mathbf{t}, \sigma^2\right)$ is a normalization constant.

Finally, to perform predictions using the model, it is necessary to evaluate $p(\widetilde{\mathbf{t}}|\mathbf{t}, \sigma^2)$, where $\widetilde{\mathbf{t}}$ indicates a set of testing data points. This distribution takes the form of a multivariate Gaussian, described by a mean vector and covariance matrix, in the form:

$$\begin{aligned} \widetilde{\mathbf{y}} &= \mathbf{D}\boldsymbol{\mu}, \\ \widetilde{\mathbf{C}} &= \sigma^2 + \mathbf{D}^{\mathrm{T}}\boldsymbol{\Sigma}\mathbf{D}, \end{aligned} \tag{26}$$

with $\boldsymbol{\mu}$ and $\boldsymbol{\Sigma}$ representing the mean vector and covariance matrix of the target. The goal of SBL-RVM is to estimate these quantities by defining the most suited weights $\boldsymbol{\gamma}$. The parameters $\boldsymbol{\mu}$ and $\boldsymbol{\Sigma}$ correspond to the optimal values obtained through the Bayesian learning process. The quantity $\widetilde{\mathbf{y}}$ and $\widetilde{\mathbf{C}}$ represent the predicted measurements derived from the optimal parameters, as expressed in Eq. (23). Through this process, the weights can be driven to zero, leaving only the significant terms. The algorithm will then determine which features are relevant for predicting the fundamental frequency. The dictionary chosen for this application is composed of the following functions:

$$\mathbf{D}(\mathbf{x}) = \begin{cases} \mathbf{x} \\ \mathbf{x}^2 \\ \nabla(\nabla(\mathbf{x})) \\ \tan \mathbf{x} \\ \log(|\mathbf{x}| + 1) \\ (1 + e^{-\mathbf{x}})^{-1} \end{cases}. \tag{27}$$

By combining the weights for the different input geometric parameters, it is possible to estimate the output (estimated frequency).

2.3.3 Feedforward neural network model (A)

Deep Neural Networks have proven to be a useful tool when dealing with regression tasks (Goodfellow et al. 2016; Minsky and Papert 2017). Here, a fully connected neural network, known as feedforward neural network, has been exploited.

Geometric properties (i.e., features) are fed to the input layer to predict the fundamental frequency, the training being obtained by means of the well-known backpropagation algorithm. To optimize the model parameters and hyperparameters, the training dataset was further subdivided into training and internal validation sets, with 75% of the data used for training and the 25% for validation. No separate test was used during this optimization phase. The input data consists of the matrix containing the geometric properties of each bell tower (H, H_{eff}, $L_{\min}$, $L_{\max}$, and s) and the network was then used to estimate the fundamental frequency ($f_{\exp}$) of the towers (output vector).

For model A, a feedforward neural network was implemented in MATLAB® having two hidden layers of 5 neurons. The network uses a single hidden layer with a *tansig* (The MathWorks Inc 2022) (hyperbolic tangent sigmoid) activation function. The output layer used a *purelin* (linear) (The MathWorks Inc 2022) activation function. The network was trained using the Bayesian Regularization backpropagation algorithm (*trainbr*) (The MathWorks Inc 2022). The training parameters were set to a maximum of 500 epochs, a minimum performance gradient of 10^{-7}, and an early stopping criterion with a maximum of 10 consecutive validation failures.

The performance plot, highlighted in Fig. 6(a), shows the evolution of the mean squared error (MSE) during the training process for both training and validation subsets, allowing the monitoring of the learning progress and the identification of possible overfitting. A decreasing and stabilizing trend of the MSE indicates that the network learns from the data without overfitting.

On the other hand, Fig. 6(b) shows the regression plot, which compares the predicted outputs of the trained network against the target values used for training. Each point represents one sample, while the perfect prediction is represented by the bisector line. The

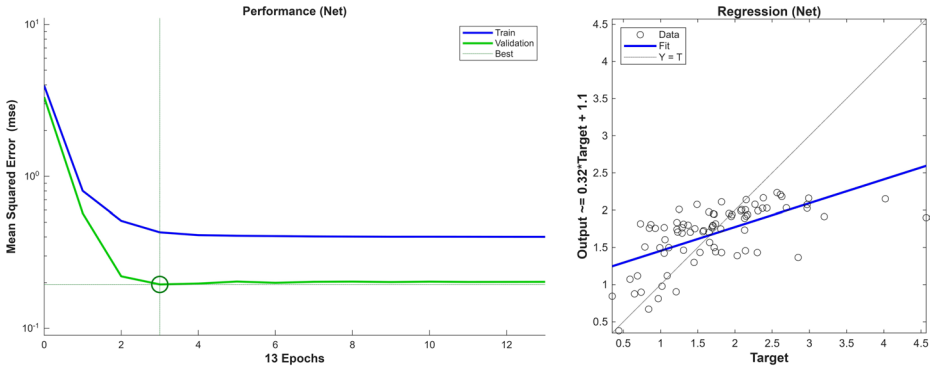

(a) (b)

Fig. 6 Performance (**a**) and regression (**b**) plots for model A. The performance plot shows the evolution of the mean squared error (MSE) during training and validation, while the regression plot compares the predicted and target values to assess the model accuracy

proximity of the data points to this line indicates the degree of alignment between predicted and observed values.

The regression plot (Fig. 6(b)) shows a rather scattered distribution of points around the bisector line, with a regression slope of approximately 0.32. This indicates a not very strong correlation between the predicted and target values, suggesting that the network was only partially able to capture the underlying relationship between the input parameters and the fundamental frequency. The dispersion of the data reflects the combined effects of the limited dataset size and the intrinsic variability of the structural properties, which constrain the model learning capability. Nevertheless, the network retains some capacity to identify the general behavior of the system.

2.3.4 Training dataset A

Training dataset A (Table 2) includes features from historic bounded masonry towers located mainly in Italy, with others located in Germany, Portugal, Spain, Greece, and the Czech Republic. Thus, these cover a broad range of European architectural typologies. These towers are characterized by geometric attributes (H, H_{eff}, $L_{\min}$, $L_{\max}$, and s), which show significant variability. The selected dataset of bounded masonry towers spans heights between 18.50 m and 112.00 m and includes single and twin towers.

The fundamental frequency of most of the towers was identified through in-situ experimental campaigns based on OMA, thus relying on ambient vibrations induced, for instance, by wind or traffic. In a limited number of towers, EMA, based on strong excitations such as seismic events or using controlled excitation sources (e.g., hammer or shaker tests), was performed to identify the fundamental frequency. In this application, the number of voters K corresponds to the experimental fundamental frequency identified under these two different operational conditions, resulting in $K=2$.

Table 3 shows the statistical measures of the dataset. In particular, experimental fundamental frequencies (f_{exp}) range from 0.35 Hz to 4.57 Hz, reflecting significant variability due to different structural configurations.

2.3.5 Validation dataset A

To validate the proposed methodology, a validation dataset consisting of features from several historic bell towers located in Italy was selected (Table 4). The dataset includes cases for which experimental measurements of the fundamental frequency are available under various structural conditions, in particular distinguishing between damaged and post-intervention scenarios.

Many towers in this dataset have experienced structural damage due to significant seismic events, notably those that occurred on May 20th and 29th, 2012, in the Emilia region (Italy), and were then subjected to structural strengthening interventions. Relevant examples include the bell tower of the Cathedral of Santa Maria Maggiore in Mirandola (Modena) (Zanotti Fragonara et al. 2017), the bell tower of the Cathedral of Santa Maria and San Giovenale in Fossano (Cuneo) (Ceravolo et al. 2016; Scussolini et al. 2023), and the bell tower of the old parish Church of S. Antonio Abate in Montà (Cuneo) (Fig. 7). Overall, the validation dataset comprises 11 experimental measurements obtained from 7 towers, capturing different structural states. The experimentally measured frequencies for these towers range between 0.68 Hz and 3.81 Hz (Table 5).

Table 2 Geometric parameters and experimental fundamental frequency of the training dataset A

T.A	Name	Country	OMA/EMA	H [m]	H_{eff} [m]	L_{min} [m]	L_{max} [m]	s [m]	f_{exp} [Hz]
1	The Soncino Civic Tower (Casciati and Al-Saleh 2010)	Italy	0	39.24	29.24	5.96	5.96	1.55	1.05
2	The San Frediano Bell Tower in Lucca (Azzara et al. 2019)	Italy	0	52.25	39.25	9.70	11.00	2.10	1.11
3	The Matilde Tower in Livorno (Zini et al. 2018)	Italy	0	29.00	19.00	12.00	12.00	2.50	2.69
4	The San Gimignano "Torre Grossa" (Bartoli et al. 2013)	Italy	1	55.81	35.76	9.50	9.50	2.60	1.31
5	Main Tower of the San Felice sul Panaro medieval fortress (Bassoli et al. 2018)	Italy	0	32.00	22.00	10.00	10.00	2.50	1.72
6	Bell tower of the historic Cathedral of Fiesole (Bru et al. 2019)	Italy	0	38.00	28.00	4.10	5.10	1.00	0.87
7	San Vittore Bell tower (Cabboi et al. 2017)	Italy	0	36.72	26.82	5.70	5.80	1.30	1.22
8	The San Silvestro Belfry (Capanna et al. 2021)	Italy	0	33.00	14.30	5.50	6.90	1.30	2.37
9	Bell Tower of Announziata in Corfù (Carone et al. 2013)	Greece	0	20.00	13.00	3.50	3.50	1.00	2.63
10	Gabbia Tower in Mantua (Saisi et al. 2015)	Italy	0	54.00	34.00	7.10	7.15	2.40	0.99
11	San Pietro Bell Tower in Perugia (Ubertini et al. 2017)	Italy	0	61.45	44.45	7.20	7.20	1.80	1.45
12	Bell tower of St.Lucia Church in Serra San Quirico (Cosenza and Iervolino 2007)	Italy	0	34.00	22.67	5.42	5.42	1.20	1.95
13	Clerigos Tower (Cunha et al. 2014)	Portugal	0	75.60	57.60	7.70	8.15	2.50	1.02
14	Bell tower of the Cathedral of Trani (Diaferio et al. 2014)	Italy	0	57.00	42.70	7.50	7.50	1.40	2.03
15	Bell tower of the Maddalena Church (Foti et al. 2012)	Italy	0	34.70	22.90	4.11	4.38	1.04	4.57
16	Sciri Tower in Perugia (Venanzi et al. 2020)	Italy	0/1	41.00	24.00	7.15	7.35	2.10	1.72/1.69
17	Bell tower of the Monza's Cathedral (Gentile and Saisi 2007)	Italy	0	74.10	54.00	10.00	10.00	1.40	0.59
18	Bell Tower di S. Maria del Carrobiolo in Monza (Gentile et al. 2019)	Italy	0	33.70	20.90	5.70	5.90	0.78	1.92

Table 2 (continued)

T.A	Name	Country	OMA/EMA	H [m]	H_{eff} [m]	L_{min} [m]	L_{max} [m]	s [m]	f_{exp} [Hz]
19	Bell Tower of the Church of Santa Justas and Rufina in Orihuela (Ivorra et al. 2010)	Spain	0	35.50	20.90	7.16	7.16	1.50	2.15
20	Bell Tower of Sra. De la Misericordia Church (Ivorra and Pallarés 2006)	Spain	0	41.00	28.00	5.60	5.60	1.20	1.29
21	Tower of University of Coimbra (Júlio et al. 2008)	Portugal	0	35.00	23.50	5.60	5.70	1.30	2.13
22	Torre del Mangia (Pieraccini et al. 2014)	Italy	0	88.00	57.00	7.00	7.00	2.50	0.35
23	The Bell Tower of Basilica dei Frari (Pavlovic et al. 2019)	Italy	0	56.60	41.60	9.20	9.40	1.40	1.05
24	Tower of the Provincial Administration Building (Foti et al. 2012)	Italy	0	60.00	33.97	9.00	9.00	2.35	2.30
25	Bell tower of Nuestra S.ra del Pilar Church (Ivorra and Cervera 2002)	Spain	1	37.19	26.50	4.68	4.68	1.45	0.73
26	Torrazzo in Cremona (Binda et al. 2000)	Italy	0	112.00	103.70	13.00	13.00	3.30	0.44
27	Bell tower of the Santa Maria del Carmine Church (Ceroni et al. 2009)	Italy	0	68.00	49.00	9.00	9.00	4.00	0.69
28	Ghirlandina Tower in Modena (Sabia et al. 2015)	Italy	0	88.82	49.00	11.00	11.00	3.90	0.74
29	San Nicolas Bell Tower (Ivorra et al. 2009)	Spain	0	42.50	28.00	6.62	6.62	1.00	0.85
30	Zuccaro's Tower (Gentile et al. 2019)	Italy	0	43.00	33.00	8.50	8.50	1.10	1.23
31	Civic Tower of the Margherita Palace (Peeters at al. 2011)	Italy	0	43.00	29.00	6.50	7.00	2.00	1.57
32	Bell Tower of S. Giorgio Church in Trignano (Bongiovanni et al. 2000)	Italy	0/1	18.50	11.00	3.00	3.35	0.40	2.70/2.43
33	Torre Aquila in Trento (Ceriotti et al. 2009)	Italy	0	31.00	20.00	4.50	7.80	0.80	1.25
34	St. Martin bell-tower of Burano (Casarin et al. 2009)	Italy	0	53.00	37.80	6.15	6.15	0.80	0.79
35	The bell tower of Santa Maria di San Luca (Colapietro et al. 2013)	Italy	0	46.00	27.00	6.25	6.25	1.50	1.40
36	Bell Tower in Santa Maria a Vico (Ferraioli et al. 2018)	Italy	0	40.00	24.70	8.30	8.30	2.00	1.31
37	Tower of the Podestà palace in Montelupone (Clementi et al. 2017)	Italy	0	27.00	14.20	6.00	6.00	2.00	1.49

Table 2 (continued)

T.A	Name	Country	OMA/EMA	H [m]	H_{eff} [m]	L_{min} [m]	L_{max} [m]	s [m]	f_{exp} [Hz]
38	Bell-tower of Santa Maria di Loreto (Diaferio et al. 2017)	Italy	0	38.30	29.30	6.30	6.30	2.00	1.69
39	Salvucci Tower (North) in San Gimignano (Bartoli et al. 2017)	Italy	0	41.50	27.50	5.20	6.00	2.00	1.22
40	Salvucci Tower (South) in San Gimignano (Bartoli et al. 2017)	Italy	0	42.80	27.30	7.10	7.20	2.30	1.58
41	Collegiata tower in San Gimignano (Bartoli et al. 2017)	Italy	0	38.80	27.60	7.00	7.30	2.00	1.70
42	Propositura Tower in San Gimignano (Bartoli et al. 2017)	Italy	0	21.00	14.00	6.70	6.70	2.20	4.02
43	Rognosa Tower in San Gimignano (Bartoli et al. 2017)	Italy	0	44.00	24.34	6.20	7.20	2.00	1.46
44	Ardinghelli Tower in San Gimignano (Bartoli et al. 2017)	Italy	0	27.60	14.90	4.30	5.40	1.40	2.97
45	Diavolo Tower in San Gimignano (Bartoli et al. 2017)	Italy	0	32.00	20.00	5.60	8.60	1.20	2.31
46	Becci Tower in San Gimignano (Bartoli et al. 2017)	Italy	0	39.40	24.40	6.30	6.50	2.30	1.37
47	Cugnanesi Tower in San Gimignano (Bartoli et al. 2017)	Italy	0	42.80	29.80	7.50	7.70	2.60	1.29
48	Coppi-Campatelli tower in San Gimignano (Bartoli et al. 2017)	Italy	0	31.00	17.00	6.40	8.20	1.50	2.97
49	Tower of Castelvecchio fortress (Furlan 2015)	Italy	0	35.20	19.51	11.84	12.20	2.44	1.71
50	Twin towers - St. Torcato church (Ramos et al. 2013)	Portugal	0	57.57	36.12	6.15	7.46	1.42	2.14
51	Funchal's Cathedral Bell Tower (Jardim et al. 2013)	Portugal	0	52.60	45.00	9.44	9.44	1.64	1.82
52	Bell tower of the Metropolitan Cathedral of Fermo (Bianconi et al. 2020)	Italy	0	48.10	23.80	9.50	10.00	2.70	1.65
53	S. Maria Bell Tower in Morrone del Sannio (Bartoli et al. 2020)	Italy	0	35.00	20.00	6.47	7.15	1.34	1.96
54	S.Maria Bell Tower in Ripabottoni (Bartoli et al. 2020)	Italy	0	27.50	15.00	4.95	5.20	1.25	2.27
55	Bell-tower of St. Nicola's church in Pisa (Beconcini and Croce 2006)	Italy	0	35.55	18.55	5.00	5.00	2.00	3.20
56	The Civic Tower of Ostra (Standoli et al. 2021)	Italy	0	30.25	20.30	7.30	7.50	1.10	2.09

Table 2 (continued)

T.A	Name	Country	OMA/EMA	H [m]	H_{eff} [m]	L_{min} [m]	L_{max} [m]	s [m]	f_{exp} [Hz]
57	Bell Tower of St. Jakub Church in Hora (Testa et al. 2023)	Czech Republic	0	86.00	66.60	9.00	10.20	2.05	0.97
58	Bell Tower of St. Jakub Church in Cirkvice (Testa et al. 2023)	Czech Republic	0	21.57	13.57	4.85	5.19	1.20	2.38
59	Lamberti Tower in Verona (Testa et al. 2023)	Italy	0	83.00	62.50	8.50	8.70	1.80	0.65
60	Bell Tower of S. Cresci in Vaglia (Bartoli et al. 2020)	Italy	0	22.00	15.00	3.59	3.67	0.98	2.15
61	Bell Tower of Sant'Agata del Mugello (Montabert et al. 2022)	Italy	0	21.00	11.00	6.00	6.30	1.10	2.61
62	Bell Tower of Palermo Cathedral (Cavaleri et al. 2019)	Italy	0	55.00	35.00	5.80	5.80	1.10	1.72
63	Bell Tower of St. Francesco Church in Amandola (Sorrentino et al. 2019)	Italy	0	33.00	18.10	5.50	5.80	0.80	2.08
64	Twin Towers - Cathedral in Magdeburg (Schmidt 2007)	Germany	0/1	101.00	82.00	14.00	42.00	3.80	0.87/0.81
65	Twin Towers - Cathedral in Halberstadt (Schmidt 2007)	Germany	0/1	91.00	60.00	10.00	26.00	2.00	1.25/1.17
66	Twin Towers - St. Johannes Church in Magdeburg (Schmidt 2007)	Germany	0/1	69.00	60.00	8.25	24.00	2.80	1.12/1.06
67	Twin Towers - St. Johannes Church in Schonebeck (Schmidt 2007)	Germany	0/1	45.00	39.00	4.00	12.10	2.00	1.09/1.03
68	Twin Towers - St. Ambrosius in Magdeburg (Schmidt 2007)	Germany	0/1	46.00	29.00	4.00	12.10	1.10	2.19/2.07
69	Twin Towers - St. Marien Cathedral in Hamburg (Schmidt 2007)	Germany	0/1	46.00	29.00	8.30	20.00	2.20	0.96/0.90
70	Twin Towers - Vockerode Church (Schmidt 2007)	Germany	0/1	32.00	24.00	4.00	12.10	1.05	1.70/1.60
71	Twin Towers - St. Nikolai Church in Quedlinburg (Schmidt 2007)	Germany	0/1	26.00	22.50	6.00	20.70	1.45	1.87/1.77
72	Twin Towers - St. Stephani in Osterwieck (Schmidt 2007)	Germany	0/1	47.00	27.50	7.40	16.00	1.70	1.86/1.76
73	Twin Towers - St. Nicolai Church in Aken (Schmidt 2007)	Germany	0/1	30.00	25.00	8.70	19.00	2.20	2.20/2.08
74	Twin Towers - St. Jakobi Church (Schmidt 2007)	Germany	0/1	61.00	46.00	8.00	28.50	1.50	1.79/1.69
75	Twin Towers - St. Marien Church in Aken (Schmidt 2007)	Germany	0/1	40.00	30.00	7.50	21.00	2.73	1.79/1.69

Table 2 (continued)

T.A	Name	Country	OMA/EMA	H [m]	H_{eff} [m]	L_{min} [m]	L_{max} [m]	s [m]	f_{exp} [Hz]
76	Twin Towers - St. George Church (Schmidt 2007)	Germany	0/1	42.00	18.00	7.00	18.00	1.55	2.24/2.10
77	Twin Towers - Martin Luther King Church in Dessau (Schmidt 2007)	Germany	0/1	26.00	24.15	5.15	9.75	1.27	2.50/2.36
78	Twin Towers - St. Stephani Church in Calbe (Schmidt 2007)	Germany	0/1	57.30	30.00	10.06	20.86	3.30	1.71/1.61
79	Twin Towers - St.Nicolai Church in Burg (Schmidt 2007)	Germany	0/1	65.00	35.00	7.30	19.20	2.00	1.59/1.47
80	Twin Towers - National Palace of Mafra (Nochebuena-Mora et al. 2021)	Portugal	0	63.80	36.60	10.11	10.11	2.18	2.85
81	Medieval Tower in Craco (Diaferio et al. 2019)	Italy	0	21.00	16.30	11.00	11.00	2.15	2.99

Table 3 Statistical properties of the training dataset A, which considers only geometric properties

Dataset A	μ	m	σ	max	min
H [m]	45.92	41.00	19.68	112.00	18.50
H_{eff} [m]	31.10	27.50	16.32	103.70	11.00
L_{max} [m]	9.92	7.50	6.40	42.00	3.35
L_{min} [m]	7.14	7.00	2.28	14.00	3.00
s [m]	1.81	1.70	0.74	4.00	0.40
f_{exp}**[Hz]**	1.72	1.69	0.77	4.57	0.35

The table reports the mean μ, the median m, the maximum max and the minimum min value of the corresponding parameter

Note: μ = mean, m = median, σ = standard deviation

Figures 8 and 9 collectively provide a correlation analysis of relationships between geometric parameters and fundamental frequencies for both training and validation datasets. Here, a scatter plot matrix illustrates the correlation among the different variables. In detail, each off-diagonal subplot displays a scatter plot comparing a pair of variables, while the diagonal subplots show the distribution of each individual variable for both training and validation sets.

These correlation and scatter plot matrices, for both training and validation datasets, reveal significant negative correlations between tower height (H and H_{eff}) and fundamental frequencies, clearly showing that taller towers exhibit lower frequencies. Conversely, base dimensions (L_{min}, L_{max}) and wall thickness (s) show weaker and more dispersed correlations, confirming their secondary role in frequency prediction. These visual and statistical analyses underscore the predominant influence of vertical dimensions on dynamic structural behavior.

Table 4 Geometric parameters and experimental fundamental frequency of the validation dataset A

V.A	Name	Country	OMA/EMA	H [m]	H_{eff} [m]	L_{min} [m]	L_{max} [m]	s [m]	f_{exp} [Hz]
1	Bell tower of the Santa Maria Maggiore Cathedral (before repair) (Zanotti Fragonara et al. 2017)	Italy	0	48.00	38.50	5.90	5.90	1.15	0.68
2	Bell tower of the Santa Maria Maggiore Cathedral (after repair) (Zanotti Fragonara et al. 2017)	Italy	0	48.00	38.50	5.90	5.90	1.15	0.79
3	Matilde bell tower of the Cathedral of San Miniato (De Stefano and Ceravolo 2007)	Italy	0	35.00	22.00	8.20	12.50	1.00	2.70
4	Bell tower of the SS. Annunziata church (before repair) (Bonato et al. 2000)	Italy	1	22.50	12.00	3.25	4.25	1.20	1.66
5	Bell tower of the SS. Annunziata church (after repair) (De Stefano and Ceravolo 2007)	Italy	0	22.50	12.00	3.25	4.25	1.20	1.97
6	S. Giovenale Bell Tower in Fossano (before repair) (Ceravolo et al. 2016)	Italy	0	46.00	31.60	9.00	9.70	1.50	1.29
7	S. Giovenale Bell Tower in Fossano (after repair)	Italy	0	46.00	31.60	9.00	9.70	1.50	1.33
8	Bell Tower of the Church "Madonnina della Neve" in Cuneo (Ceravolo et al. 2016)	Italy	0	13.00	7.10	1.50	1.50	0.60	3.81
9	Bell tower of the Church of Santa Caterina in Collegnago (Ceravolo et al. 2017)	Italy	0/1	19.30	9.00	3.80	3.80	0.70	1.97/1.82
10	Bell tower of the old parish church of S. Antonio Abate (before repair)	Italy	0	17.35	10.76	2.70	2.70	0.57	2.17
11	Bell tower of the old parish church of S. Antonio Abate (after repair)	Italy	0	17.35	10.76	2.70	2.70	0.57	2.36

2.4 Estimation of the fundamental frequency for historic bounded masonry towers through geometric and mechanical parameters (B)

Here, the PL model is evaluated by combining both geometric and mechanical parameters. The estimation of mechanical parameters, such as the Young's modulus E and the material density ρ, is inherently subject to greater uncertainty compared to geometric properties. This arises from the variability in both the sources of information and the methods used for their assessment. In the present study, mechanical properties were obtained from a combination of sources, including measurements reported in previous studies, visual inspections, non-destructive testing techniques, and calibrated numerical models based on experimental data. Each of these approaches presents differing levels of reliability, and their integration results in a heterogeneous dataset that reflects both the diversity and the limitations of the available information. By combining multiple predictive formulations, the aim of the framework is to

(a) (b) (c)

Fig. 7 Historic bell towers of (**a**) the cathedral of Santa Maria Maggiore in Mirandola (Modena, Italy), (**b**) the cathedral of Santa Maria and San Giovenale in Fossano (Cuneo, Italy), (**c**) the old parish church of S. Antonio Abate in Montà (Cuneo, Italy)

Table 5 Statistical properties of the validation dataset A, which considers only geometric properties

Dataset A	μ	m	σ	max	min
H [m]	30.45	22.50	14.21	48.00	13.00
H_{eff} [m]	20.35	12.00	12.42	38.50	7.10
L_{max} [m]	5.72	4.25	3.49	12.50	1.50
L_{min} [m]	5.02	3.80	2.72	9.00	1.50
s [m]	1.01	1.15	0.35	1.50	0.57
f_{exp}**[Hz]**	1.88	1.90	0.90	3.81	0.68

The table reports the mean μ, the median m, the maximum max and the minimum min value of the corresponding parameter

Note: μ = mean, m = median, σ = standard deviation

mitigate the influence of uncertainties in the mechanical parameters, leading to more stable and reliable estimates across a range of tower geometries and material conditions.

The five candidates selected for analysis B are represented by (i) three empirical formulations from literature, (ii) a neural network, and (iii) a SBL model. Given the scarcity of empirical laws based on geometric and mechanical parameters, data-driven models (i.e., neural network and SBL) are added to explicitly explore relationships between mechanical and geometric features reflected in the fundamental frequency of the bounded masonry bell towers.

Also here, the terms “training” and “validation” are used for consistency with the previous sections. As before, they simply refer to the reference subsets in the case of empirical

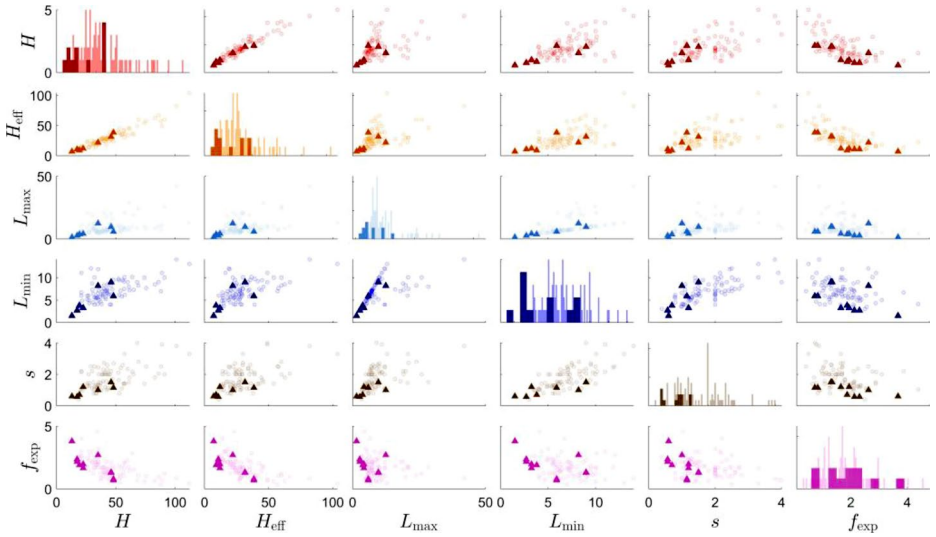

Fig. 8 Scatter plot matrix of geometric parameters and fundamental frequency for the training and validation sets of dataset A. The diagonal panels display the univariate distributions (histograms) of each variable, while off-diagonal scatter plots highlight possible correlations and interdependencies among parameters. Light-colored circles represent the training data, while dark-colored triangles indicate the validation data

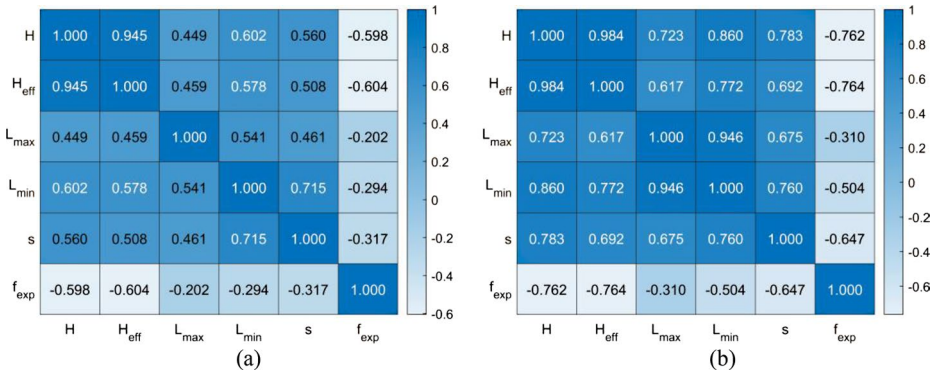

Fig. 9 Correlation matrix of geometric parameters and fundamental frequency for (**a**) training and (**b**) validation set A. The matrices display the correlation coefficients among the geometric variables and the experimental fundamental frequency. The color scale ranges from −1 (strong negative correlation, light tones) to+1 (strong positive correlation, dark blue), quantifying the degree of correlation between each pair of parameters

Table 6 Empirical laws (candidates) for predicting the fundamental frequency based on geometric and mechanical parameters

Reference	Equation (f_1 $[Hz]$)	
Shakya et al. (2016)	$\frac{1.875^2}{2\pi H^2}\sqrt{\frac{1.375EJ}{\rho A}}$	(28)
Bartoli et al. (2017) (a)	$\frac{0.2a}{H_{eff}^2}(1-n)\,v_p$	(29)
Bartoli et al. (2017) (b)	$\frac{0.15a}{H_{eff}^2}v_p$	(30)

The table summarizes the three empirical formulations selected from the literature and used as candidate estimation laws in the proposed framework. The formulations include parameters such as H, H_{eff}, L_{min}, L_{max}, E, and ρ

laws, while for the SBL and neural network models they correspond to the actual training-validation/testing procedure required by the models.

2.4.1 Fundamental frequency estimation laws (B)

The three empirical formulations chosen for this analysis (Table 6), which comprise geometric and mechanical parameters as input data, are:

- Shakya et al. (2016), which consider H, E and ρ.
- Two different laws from Bartoli et al. (2017), one (a) including H_{eff} , n and v_p, which consider both E and ρ, and the other (b) which does not consider n as input parameter, but assumes it to be constant.

2.4.2 Sparse Bayesian learning model (B)

The creation of the SBL model for analysis B involves the use of the same dictionary used for model A, composed of the following functions:

$$\mathbf{D}(\mathbf{x}) = \begin{cases} \mathbf{x} \\ \mathbf{x}^2 \\ \nabla(\nabla(\mathbf{x})) \\ \tan\mathbf{x} \\ \log(|\mathbf{x}|+1) \\ (1+e^{-\mathbf{x}})^{-1} \end{cases}. \tag{31}$$

The fundamental frequency of the masonry towers can be estimated by linearly combining the weights with the target function associated with the input geometric and mechanical parameters.

2.4.3 Feedforward neural network model (B)

Building upon the setup described for case A (Sect 2.3.3), a feedforward neural network (Net) is developed to predict experimentally measured fundamental frequency (f_{exp}) starting from geometric and mechanical parameters. The network architecture (model B), training strategy, and activation functions were kept identical, while the input matrix was expanded to incorporate material properties (E and ρ) alongside geometric parameters (H, H_{eff}, L_{min},

L_{max}, s). The dataset was again divided into training and internal validation subsets, with a 75% for training and 25% for validation. In the same way, the performance and regression plots are shown in Fig. 10(a) and 10(b), respectively.

The regression results (Fig. 10(b)) reveal an improvement compared to the previous case, with a regression slope of about 0.53 and a clearer alignment of the predicted values with the target trend. Although the correlation is still moderate, the model shows a better performance. The reduced scatter suggests that the inclusion of additional input information (i.e., mechanical properties) contributed to stabilizing the learning process. However, the variability of the available data and the relatively small number of samples still limit the network performance.

2.4.4 Training dataset B

Training dataset B (Table 7) includes 47 historic masonry towers characterized by both geometric and mechanical parameters. In detail, the dataset comprises H, H_{eff}, L_{min}, L_{max}, s, E, and ρ. The training dataset B is smaller than dataset A, as it includes only those towers for which both types of information are available. Also here, as in the previous case concerning only geometric parameters, the number of voters K corresponds to the experimental fundamental frequency identified through OMA and EMA (based on strong excitations), meaning $K = 2$. The experimentally measured fundamental frequency (f_{exp}) within this dataset range from 0.35 Hz to 4.02 Hz, showing significant variability due to geometric and mechanical properties of the structures. Detailed statistical measures of the training dataset B are summarized in Table 8.

2.4.5 Validation dataset B

Validation dataset B (Table 9) considers the same historic masonry bell towers located in Italy used in validation dataset A, for which mechanical properties were available. This dataset includes all the geometric properties, in addition to E and ρ. Maintaining the same validation dataset allows a straightforward comparison between analyses A and B, isolating

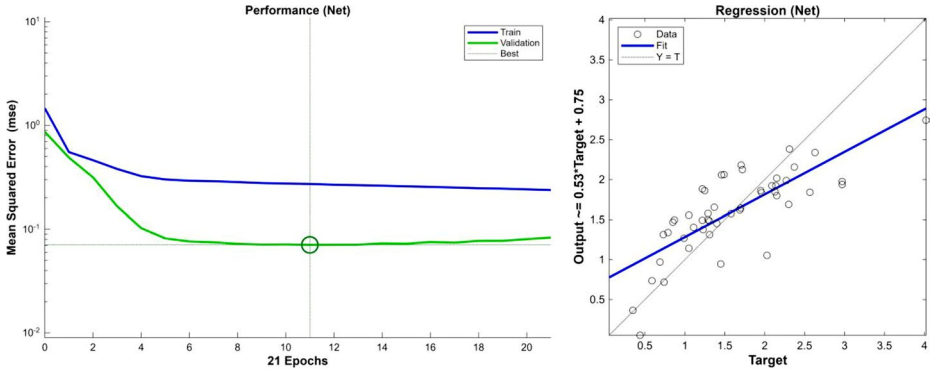

Fig. 10 Performance (**a**) and regression (**b**) plots for model B. The performance plot shows the evolution of the mean squared error (MSE) during training and validation, while the regression plot compares the predicted and target values to assess the model accuracy

Table 7 Geometric and mechanical parameters and experimental fundamental frequency of the training dataset B

T.B	Name	Country	OMA/ EMA	H [m]	H_{eff} [m]	L_{min} [m]	L_{max} [m]	s [m]	E [MPa]	ρ [kg/m^3]	f_{exp} [Hz]
1	The Soncino Civic Tower (Casciati and Al-Saleh 2010)	Italy	0	39.24	29.24	5.96	5.96	1.55	1600.0	1834.0	1.05
2	The San Frediano Bell Tower in Lucca (Azzara et al. 2019)	Italy	0	52.25	39.25	9.70	11.00	2.10	1800.0	1837.0	1.11
3	The San Gimignano "Torre Grossa" (Bartoli et al. 2013)	Italy	1	55.81	35.76	9.50	9.50	2.60	3000.0	1800.0	1.31
4	Main Tower of the San Felice sul Panaro medieval fortress (Bassoli et al. 2018)	Italy	1	32.00	22.00	10.00	10.00	2.50	1500.0	1836.0	1.72
5	Bell tower of the historic Cathedral of Fiesole (Bru et al. 2019)	Italy	0	38.00	28.00	4.10	5.10	1.00	2000.0	1835.0	0.87
6	San Vittore Bell tower (Cabboi et al. 2017)	Italy	0	36.72	26.82	5.70	5.80	1.30	1500.0	2037.0	1.22
7	The San Silvestro Belfry (Capanna et al. 2021)	Italy	0	33.00	14.30	5.50	6.90	1.30	3540.0	2000.0	2.37
8	Bell Tower of Annunziata in Corfù (Carone et al. 2013)	Greece	0	20.00	13.00	3.50	3.50	1.00	1340.0	2037.0	2.63
9	Gabbia Tower in Mantua (Saisi et al. 2015)	Italy	0	54.00	34.00	7.10	7.15	2.40	1700.0	1833.0	0.99
10	San Pietro Bell Tower in Perugia (Ubertini et al. 2017)	Italy	0	61.45	44.45	7.20	7.20	1.80	1800.0	1837.0	1.45
11	Bell tower of St.Lucia Church in Serra San Quirico (Cosenza and Iervolino 2007)	Italy	0	34.00	22.67	5.42	5.42	1.20	1500.0	1937.0	1.95
12	Bell tower of the Cathedral of Trani (Diaferio et al. 2014)	Italy	0	57.00	42.70	7.50	7.50	1.40	2200.0	1835.0	2.03
13	Sciri Tower in Perugia (Venanzi et al. 2020)	Italy	0/1	41.00	24.00	7.15	7.35	2.10	5770.0	2200.0	1.72/1.69
14	Bell tower of the Monza's Cathedral (Gentile and Saisi 2007)	Italy	0	74.10	54.00	10.00	10.00	1.40	1600.0	1834.0	0.59
15	Bell Tower of the Church of Santa Justas and Rufina in Orihuela (Ivorra et al. 2010)	Spain	0	35.50	20.90	7.16	7.16	1.50	1400.0	1800.0	2.15
16	Bell Tower of Sra. De la Misericordia Church (Ivorra and Pallarés 2006)	Spain	0	41.00	28.00	5.60	5.60	1.20	2000.0	1835.0	1.29
17	Tower of University of Coimbra (Júlio et al 2008)	Portugal	0	35.00	23.50	5.60	5.70	1.30	3000.0	1935.0	2.13
18	Torre del Mangia (Pieraccini et al. 2014)	Italy	0	88.00	57.00	7.00	7.00	2.50	2000.0	1835.0	0.35
19	The Bell Tower of Basilica dei Frari (Pavlovic et al. 2019)	Italy	0	56.60	41.60	9.20	9.40	1.40	2200.0	1800.0	1.05
20	Tower of the Provincial Administration Building (Foti et al. 2012)	Italy	0	60.00	33.97	9.00	9.00	2.35	2525.0	2198.0	2.30
21	Bell tower of Nuestra S.ra del Pilar Church (Ivorra and Cervera 2002)	Spain	1	37.19	26.50	4.68	4.68	1.45	1100.0	1632.0	0.73
22	Torrazzo in Cremona (Binda et al. 2000)	Italy	0	112.00	103.70	13.00	13.00	3.30	2000.0	1800.0	0.44
23	Bell tower of the Santa Maria del Carmine Church (Bongiovanni et al. 2000)	Italy	0	68.00	49.00	9.00	9.00	4.00	850.0	1833.0	0.69
24	Ghirlandina Tower in Modena (Sabia et al. 2015)	Italy	0	88.82	49.00	11.00	11.00	3.90	1700.0	1833.0	0.74
25	San Nicolas Bell Tower (Ivorra et al. 2009)	Spain	0	42.50	28.00	6.62	6.62	1.00	1500.0	1800.0	0.85
26	Zuccaro's Tower in Mantua (Gentile et al. 2019)	Italy	0	43.00	33.00	8.50	8.50	1.10	3200.0	1700.0	1.23
27	Bell Tower of S. Giorgio Church in Trignano (Bongiovanni et al. 2000)	Italy	0/1	18.50	11.00	3.00	3.35	0.40	700.0	1631.0	2.70/2.43
28	Torre Aquila in Trento (Ceriotti et al. 2009)	Italy	0	31.00	20.00	4.50	7.80	0.80	1100.0	1836.0	1.25
29	St. Martin bell-tower of Burano (Casarin et al. 2009)	Italy	0	53.00	37.80	6.15	6.15	0.80	2300.0	2039.0	0.79
30	The bell tower of Santa Maria di San Luca (Colapietro et al. 2013)	Italy	0	46.00	27.00	6.25	6.25	1.50	1900.0	1833.0	1.40
31	Bell Tower in Santa Maria a Vico (Ferraioli et al. 2018)	Italy	0	40.00	24.70	8.30	8.30	2.00	2400.0	1600.0	1.31

Table 7 (continued)

T.B	Name	Country	OMA/EMA	H [m]	H_{eff} [m]	L_{min} [m]	L_{max} [m]	s [m]	E [MPa]	ρ [kg/m^3]	f_{exp} [Hz]
32	Tower of the Podestà palace in Montelupone (Clementi et al. 2017)	Italy	0	27.00	14.20	6.00	6.00	2.00	1500.0	1800.0	1.49
33	Bell-tower of Santa Maria di Loreto (Diaferio et al. 2017)	Italy	0	38.30	29.30	6.30	6.30	2.00	1500.0	1836.0	1.69
34	Salvucci Tower (North) in San Gimignano (Bartoli et al. 2017)	Italy	0	41.50	27.50	5.20	6.00	2.00	2300.0	1800.0	1.22
35	Salvucci Tower (South) in San Gimignano (Bartoli et al. 2017)	Italy	0	42.80	27.30	7.10	7.20	2.30	2300.0	1800.0	1.58
36	Collegiata tower in San Gimignano (Bartoli et al. 2017)	Italy	0	38.80	27.60	7.00	7.30	2.00	2600.0	1800.0	1.70
37	Propositura Tower in San Gimignano (Bartoli et al. 2017)	Italy	0	21.00	14.00	6.70	6.70	2.20	1800.0	2200.0	4.02
38	Rognosa Tower in San Gimignano (Bartoli et al. 2017)	Italy	0	44.00	24.34	6.20	7.20	2.00	2300.0	2200.0	1.46
39	Ardinghelli Tower in San Gimignano (Bartoli et al. 2017)	Italy	0	27.60	14.90	4.30	5.40	1.40	2000.0	1800.0	2.97
40	Diavolo Tower in San Gimignano (Bartoli et al. 2017)	Italy	0	32.00	20.00	5.60	8.60	1.20	2800.0	2200.0	2.31
41	Becci Tower in San Gimignano (Bartoli et al. 2017)	Italy	0	39.40	24.40	6.30	6.50	2.30	2300.0	1800.0	1.37
42	Cugnanesi Tower in San Gimignano (Bartoli et al. 2017)	Italy	0	42.80	29.80	7.50	7.70	2.60	2300.0	1800.0	1.29
43	Coppi-Campatelli tower in San Gimignano (Bartoli et al. 2017)	Italy	0	31.00	17.00	6.40	8.20	1.50	2600.0	1800.0	2.97
44	S. Maria Bell Tower in Morrone del Sannio (Bartoli et al. 2020)	Italy	0	35.00	20.00	6.47	7.15	1.34	1230.0	1833.0	1.96
45	S.Maria Bell Tower in Ripabottoni (Bartoli et al. 2020)	Italy	0	27.50	15.00	4.95	5.20	1.25	1100.0	1836.0	2.27
46	The Civic Tower of Ostra (Standoli et al. 2021)	Italy	0	30.25	20.30	7.30	7.50	1.10	1800.0	1800.0	2.09
47	Bell Tower of S. Cresci in Vaglia (Bartoli et al. 2020)	Italy	0	22.00	15.00	3.59	3.67	0.98	1400.0	1836.0	2.15

Table 8 Statistical properties of the training dataset B, which includes geometric and mechanical properties

Dataset B	μ	m	σ	max	min
H [m]	44.23	39.70	18.53	112.00	18.50
H_{eff} [m]	29.62	27.15	15.50	103.70	11.00
L_{max} [m]	7.19	7.16	1.95	13.00	3.35
L_{min} [m]	6.79	6.44	2.02	13.00	3.00
s [m]	1.74	1.50	0.75	4.00	0.40
E [MPa]	2087	1950	972	5770	700
ρ [kg/m^3]	1881	1834	170	2500	1600
f_{exp}**[Hz]**	1.60	1.46	0.74	4.02	0.35

The table reports the mean μ, the median m, the maximum max and the minimum min value of the corresponding parameter

Note: μ = mean, m = median, σ = standard deviation

the contribution of mechanical parameters to the model predictive performance. The experimentally measured fundamental frequency (f_{exp}) ranges from 0.68 Hz to 3.81 Hz. Statistical measures for this validation dataset are provided in Table 10.

Figure 11 and Fig. 12 illustrate the correlation and relationships among the chosen geometric and mechanical parameters and the experimental fundamental frequency for both training and validation datasets B. The correlation matrices (Fig. 12) highlight, as for dataset A, strong negative correlations between tower height and experimental frequency, with correlation coefficient consistently below −0.6 for the training dataset and below −0.8 for the validation dataset. Base dimensions and wall thickness demonstrate moderate negative correlations with the frequency, suggesting that these parameters also contribute, albeit to a lesser degree, to fundamental frequency prediction. Mechanical properties show diverse degrees of correlation: E exhibits moderate negative correlation in the training dataset, whereas ρ reveals minimal or negligible correlation, particularly in the training dataset. The scatter plot matrix (Fig. 11) visually supports these values, clearly showing the inverse relationship between height and frequency. The distributions further reveal the complexity and variability of the relationship involving mechanical parameters.

3 Results and discussion

This section presents and discusses the results obtained from the application of the proposed methodology. Section 3.1 focuses on the prediction performance achieved using only geometric parameters. Section 3.2 extends the analysis by including mechanical parameters. Finally, Section 3.3 discusses the applicability and practical implications of the proposed approach, highlighting its potential for real-world implementation and its limitations.

3.1 Prediction based on geometric parameters

As a first step, the fundamental frequency for dataset A is estimated using geometric parameters only. Eight predictive models are evaluated, and their outputs are combined using the RA approach via the PL model, using four different weighting strategies. Figure 13 compares the experimental fundamental frequencies (f_{exp}) with the predictions from each candidate model, plotted against tower height H for visualization purposes in both training and validation datasets. By observing Fig. 13, most candidates show a tendency to under-

Table 9 Geometric and mechanical parameters and experimental fundamental frequency of the validation dataset B

V.B	Name	Country	OMA/EMA	H [m]	H_{eff} [m]	L_{min} [m]	L_{max} [m]	s [m]	E [MPa]	ρ [kg/m^3]	f_{exp} [Hz]
1	Bell tower of the Santa Maria Maggiore Cathedral (before repair) (Zanotti Fragonara et al. 2017)	Italy	0	48.00	38.50	5.90	5.90	1.15	1500.0	1800.0	0.68
2	Bell tower of the Santa Maria Maggiore Cathedral (after repair) (Zanotti Fragonara et al. 2017)	Italy	0	48.00	38.50	5.90	5.90	1.15	1500.0	1800.0	0.79
3	Bell tower of the SS. Annunziata church (before repair) (Bonato et al. 2000)	Italy	0	22.50	12.00	3.25	4.25	1.20	970.0	1935.0	1.66
4	Bell tower of the SS. Annunziata church (after repair) (De Stefano and Ceravolo 2007)	Italy	1	22.50	12.00	3.25	4.25	1.20	970.0	1935.0	1.97
5	S. Giovenale Bell Tower in Fossano (before repair) (Ceravolo et al. 2016)	Italy	0	46.00	31.60	9.00	9.70	1.50	1933.0	2000.0	1.29
6	S. Giovenale Bell Tower in Fossano (after repair)	Italy	0	46.00	31.60	9.00	9.70	1.50	1933.0	2000.0	1.33
7	Bell Tower of the Church “Madonnina della Neve” in Cuneo (Ceravolo et al. 2016)	Italy	0	13.00	7.10	1.50	1.50	0.60	790.0	1700.0	3.81
8	Bell tower of the Church of Santa Caterina in Collegnago (Ceravolo et al. 2017)	Italy	0/1	19.30	9.00	3.80	3.80	0.70	2055.0	2200.0	1.97/1.82
9	Bell tower of the old parish church of S. Antonio Abate (before repair)	Italy	0	17.35	10.76	2.70	2.70	0.57	1032.0	2241.0	2.17
10	Bell tower of the old parish church of S. Antonio Abate (after repair)	Italy	0	17.35	10.76	2.70	2.70	0.57	1032.0	2241.0	2.36

estimate the fundamental frequency of shorter towers. Here, results from both training and validation datasets are reported. Based on the PL model, the reference ranking list is shown in Table 11, while Figs. 14 and 15 report the average prediction error for each model considering training and validation datasets, respectively. Candidates are ordered from left to right according to their ranking, from highest to lowest. The mean value and the coefficient of variation (CV) of the error, the latter computed as the ratio between the standard deviation and the mean value, have been used as statistical quantities representing the performance of each estimation law.

It is important to note how both Net and SBL are ranked in the first positions, although they show medium-to-high mean errors in the validation dataset. This occurs because, although both models are trained on an independent dataset, this is not sufficient to generalize all outputs in the validation set. This difference mainly arises from the characteristics of the validation dataset rather than from model overfitting, as it includes towers with similar geometric and mechanical properties but significant different natural frequencies due to variations in structural health and data acquisition analysis. The lower accuracy mainly reflects the variability of the experimental data. The same can be noticed for the RA results, where mean errors in validation are higher than the ones obtained in the training phase. In this analysis, although RA does not outperform all candidates, it effectively combines knowledge (predictions) from models that, even when trained on the given dataset (e.g., Net and SBL), do not yield the lowest mean error. The different RA weighting strategies show consistent behavior between the training and validation sets, with the MRR and the linear strategy showing slightly better performance. In Fig. 16, the RA predictions are plotted against the experimental data for both training and validation datasets. The RA models exhibit consistent CV across both datasets, highlighting a consistent prediction stability.

An outlier analysis was also carried out to evaluate the behavior of the estimation laws where the prediction error is highest. This analysis aims to highlight the cases in which the models exhibit the largest error from the experimental fundamentals frequency. The upper 25% of the predictions showing the largest error from the experimental values were identified as outliers for each model and RA configuration. The corresponding error distributions of the bell tower belonging to the training dataset of the RA are shown in Figs. 17 and 18.

3.2 Geometric and mechanical parameters based results

This section presents the results of the RA strategy when applied to laws and models including both geometric and mechanical parameters (Section 2.4).

In detail, Fig. 19 shows a comparison between the experimental fundamental frequency and the corresponding predictions from each of the five candidates, plotted as a function of H. These candidates are then ranked through the PL model (Table 12). The mean error and the CV for each candidate is shown in Fig. 20 (training) and Fig. 21 (validation), together with the results obtained with the RA approach. The candidates are ordered from left to right based on their ranking position. Although SBL demonstrates good results in the training phase (mean error: 21.13%), the RA predictions achieve a good performance, with the best result for the exponential decay weighting strategy, with a mean error of 20.83% in this phase. The RA outcome outperforms all the candidates in the validation phase, with different results based on the weighting strategy. The best results are achieved with the MRR and linear weighting strategies with a mean error of 16.36% and 14.74%, respectively.

Table 10 Statistical properties of the validation dataset B, which includes geometric and mechanical properties

Dataset B	μ	m	σ	max	min
H [m]	30.00	22.50	14.89	48.00	13.00
H_{eff} [m]	20.18	12.00	13.08	38.50	7.10
L_{max} [m]	5.04	4.25	2.81	9.70	1.50
L_{min} [m]	4.70	3.53	2.65	9.00	1.50
s [m]	1.01	1.15	0.37	1.50	0.57
E [MPa]	1372	1266	474	2055	790
ρ [kg/m^3]	1985	1968	192	2241	1700
f_{exp}**[Hz]**	1.80	1.78	0.90	3.81	0.68

The table reports the mean μ, the median m, the maximum max and the minimum min value of the corresponding parameter

Note: μ = mean, m = median, σ = standard deviation

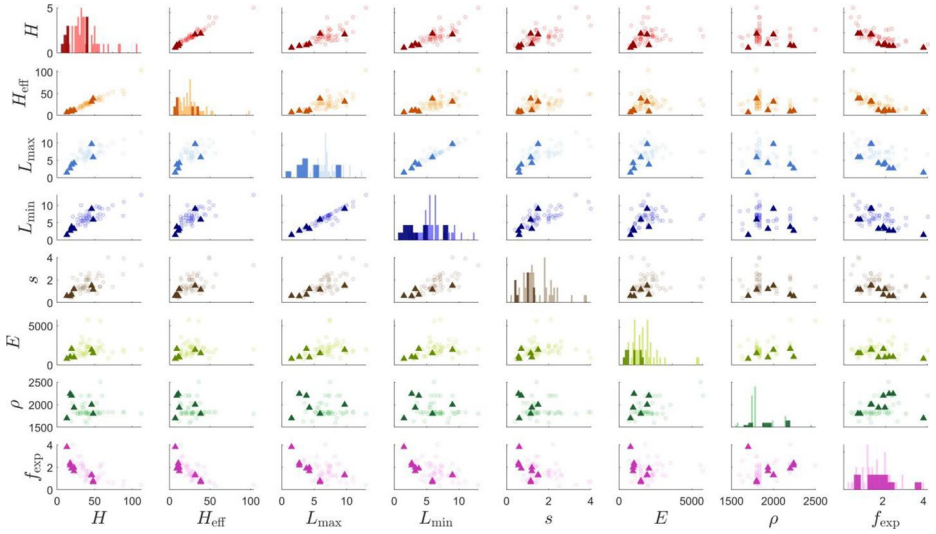

Fig. 11 Scatter plot matrix of geometric and mechanical parameters and fundamental frequency for the training and validation sets of dataset B. The diagonal panels display the univariate distributions (histograms) of each variable, while off-diagonal scatter plots highlight possible correlations and interdependencies among parameters light-colored circles represent the training data, while dark-colored triangles indicate the validation data

Finally, Fig. 22 shows the direct RA predictions derived from the different weighting strategies vs. the experimental fundamental frequencies. The high level of accuracy between estimated and observed values highlights the benefits of using RA approach to produce accurate predictions across a broad range of parameters that characterize historic bounded masonry towers.

The improved performance can be found in the core philosophy of the RA method: rather than relying on a single model, RA shares information from multiple candidates. By doing so, it effectively captures a wider spectrum behavior represented in the individual candidates (e.g., prediction models). The weighting strategies further ensure the model to assign greater influence to predictions coming from higher-ranked candidates, while retaining contributions from the whole set of candidates where a threshold is not defined, or the weight decay

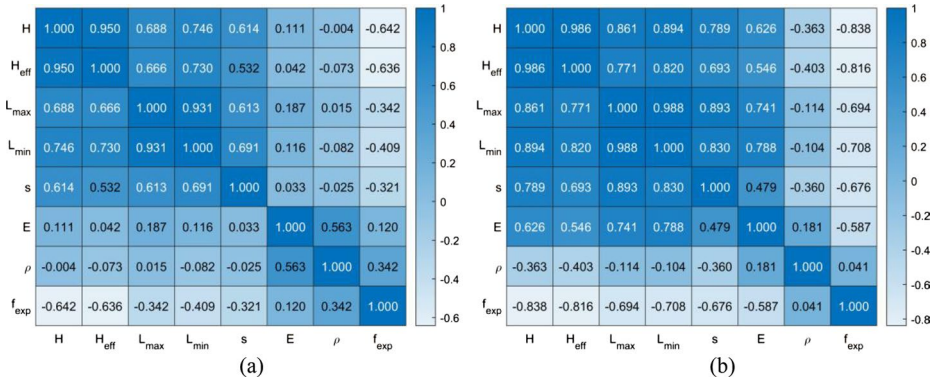

Fig. 12 Correlation matrix of geometric and mechanical parameters vs. fundamental frequency for (**a**) training and (**b**) validation set B. The matrices display the correlation coefficients among the geometric and mechanical variables and the experimental fundamental frequency. The color scale ranges from −1 (strong negative correlation, light tones) to + 1 (strong positive correlation, dark blue), quantifying the degree of correlation between each pair of parameters

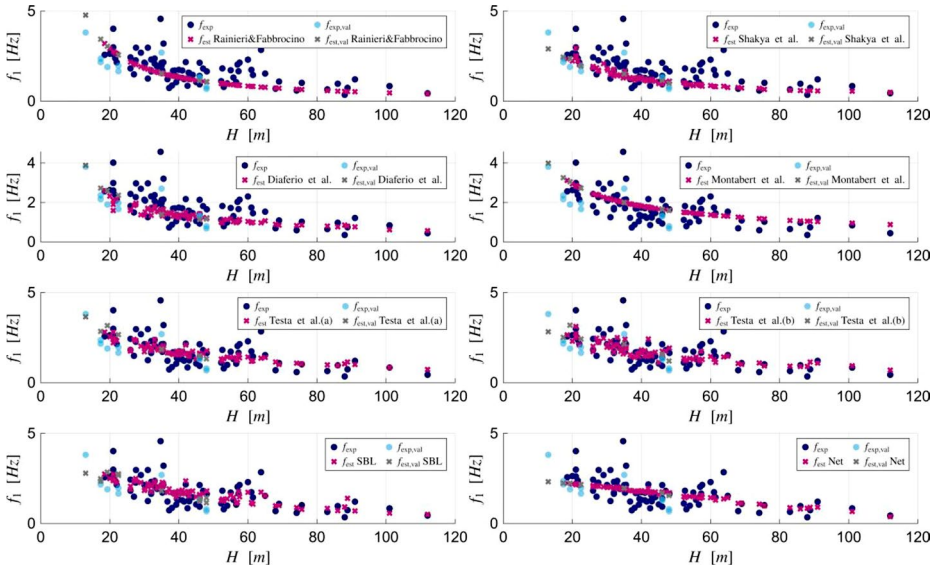

Fig. 13 Dataset A (geometric parameters): comparison between estimated and experimental fundamental frequencies of masonry towers as a function of the total height *H* for each candidate model. Dark blue circles represent the experimental fundamental frequency for the training dataset, while light blue circles denote those of the validation dataset. Magenta crosses indicate the frequency estimated by each candidate model for the training data, and grey crosses represent the corresponding estimates for the validation set

is not very high. When both geometric and mechanical information are available, results demonstrate that RA can be a good solution for estimating the fundamental frequency of historic bounded masonry towers. Here, the RA predictive model exhibits low dispersion in fitting the experimental frequencies. This approach can be exploited to assess the seismic behavior of masonry bell towers, allowing for the evaluation of their dynamic properties

Table 11 Dataset A (geometric parameters): reference ranking list for candidates based on geometric parameters

P	1st	2nd	3rd	4th	5th	6th	7th	8th
266	SBL	Montabert et al. (2023)	Net	Testa et al. (2024) (a)	Testa et al. (2024) (b)	Diaferio et al. (2018)	Rainieri and Fabbrocino (2011)	Shakya et al. (2016)

The number p represents the row of the permutation matrix $\mathbf{C}$ which describes the best ranking

using only a few available input parameters. Although the first and second ranked models developed on this specific dataset exhibit strong results (i.e., SBL and Net), they show worse results in the validation dataset. The proposed RA approach not only exceeds their performance but also offers higher generalization, making it valid to fundamental frequency estimation of different towers beyond the original dataset.

The inclusion of mechanical parameters in the laws, despite their variability, consistently improves the estimation of the fundamental frequency. This indicates that even when mechanical properties are affected by uncertainty, they provide complementary information that enhances the performance of the models. The RA framework further contributes to this by integrating models based on different combinations of geometric and mechanical parameters. This approach ensures that the methodology continues to work in scenarios where some mechanical information may be incomplete or approximate. It also demonstrates the advantage of using both experimental mechanical data and, where the latter is not available for certain towers, calibrated models to provide more accurate predictions.

As shown in Fig. 20, the RA technique consistently outperforms the individual SBL and Net models, even though these were specifically trained and optimized using the same dataset adopted for the RA calibration. This confirms that the RA process is able to leverage the heterogeneity of the included models rather than favoring any single one. Overall, this outcome supports the idea that the RA framework not only mitigates potential bias due to shared training data, but also improves the estimations by exploiting the complementary nature of empirical and data-driven knowledge sources.

Also here, an outlier analysis has been performed to identify the upper 25% of the predictions showing the largest errors from the experimental values coming from the training dataset of the RA. The corresponding error distributions are shown in Figs. 23 and 24. The error values follow the ranking list, with lower mean error of the outliers related to the SBL and Net.

3.3 Applicability and practical implications of the proposed method

The presented framework integrates empirical laws, feedforward neural networks, and SBL models through a RA approach, offering a comprehensive strategy for estimating the fundamental frequency of historic bounded masonry towers. The RA method combines the knowledge embedded in different estimation laws to provide a unified and statistically consistent and stable result. It involves identifying the combination of estimation tools (e.g., empirical laws and data-driven models) that simultaneously satisfy two key conditions: (i) they are associated with the most plausible ranking list, meaning the permutation with the highest likelihood of being observed (maximum likelihood criterion); and (ii) they yield results across the different estimation tools that are in the highest possible agreement, quantified by the lowest observed variance.

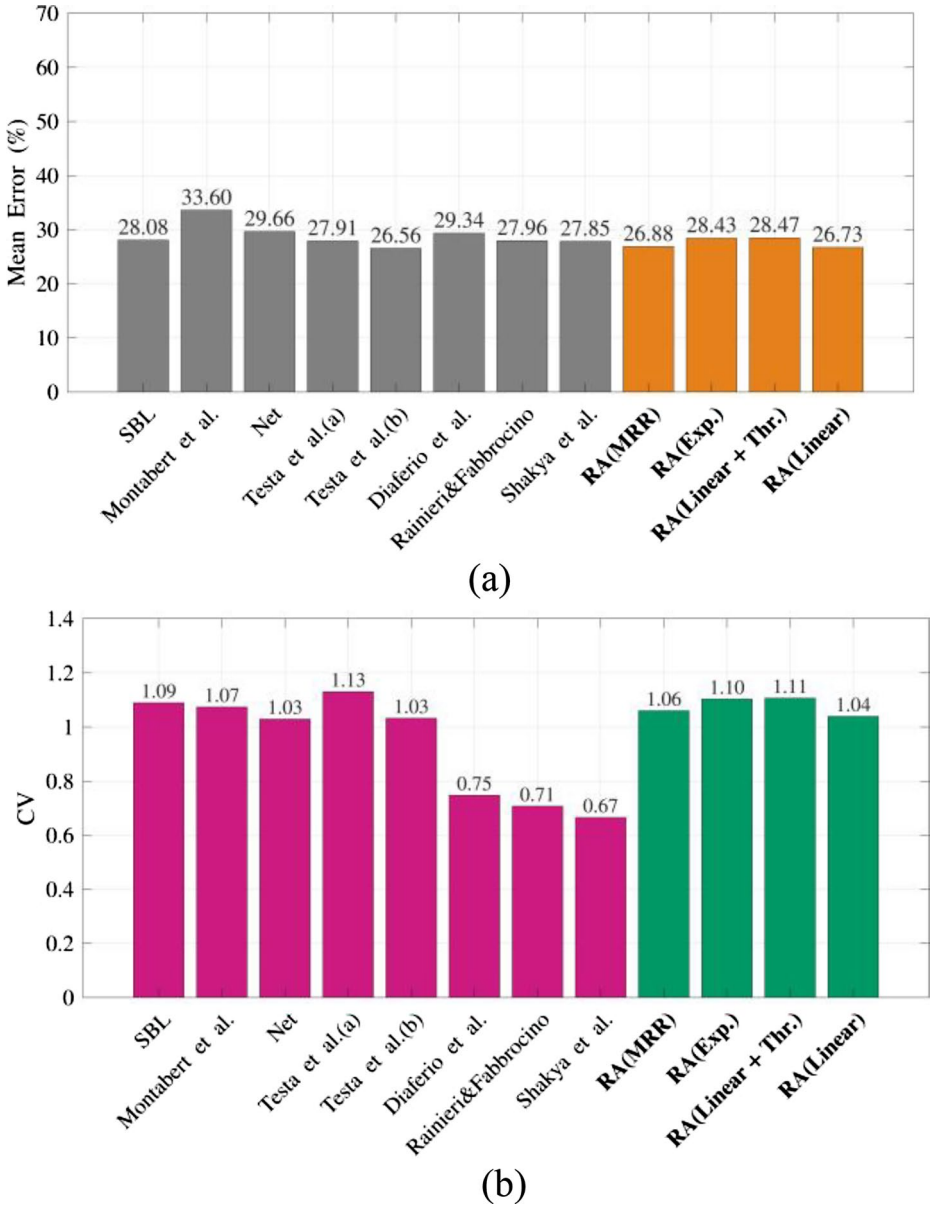

Fig. 14 Training dataset A (geometric parameters): (**a**) mean prediction error for different candidate models (grey) and different RA weighting strategies (orange); (**b**) coefficient of variation for different candidate models (magenta) and different RA weighting strategies (green)

- A key strength of the proposed methodology lies in its ability to share information from diverse estimation tools, allowing it to provide reliable frequency estimates even for previously untested or poorly documented towers. By integrating the predictions of both empirical and data-driven formulations, the RA approach can effectively perform a

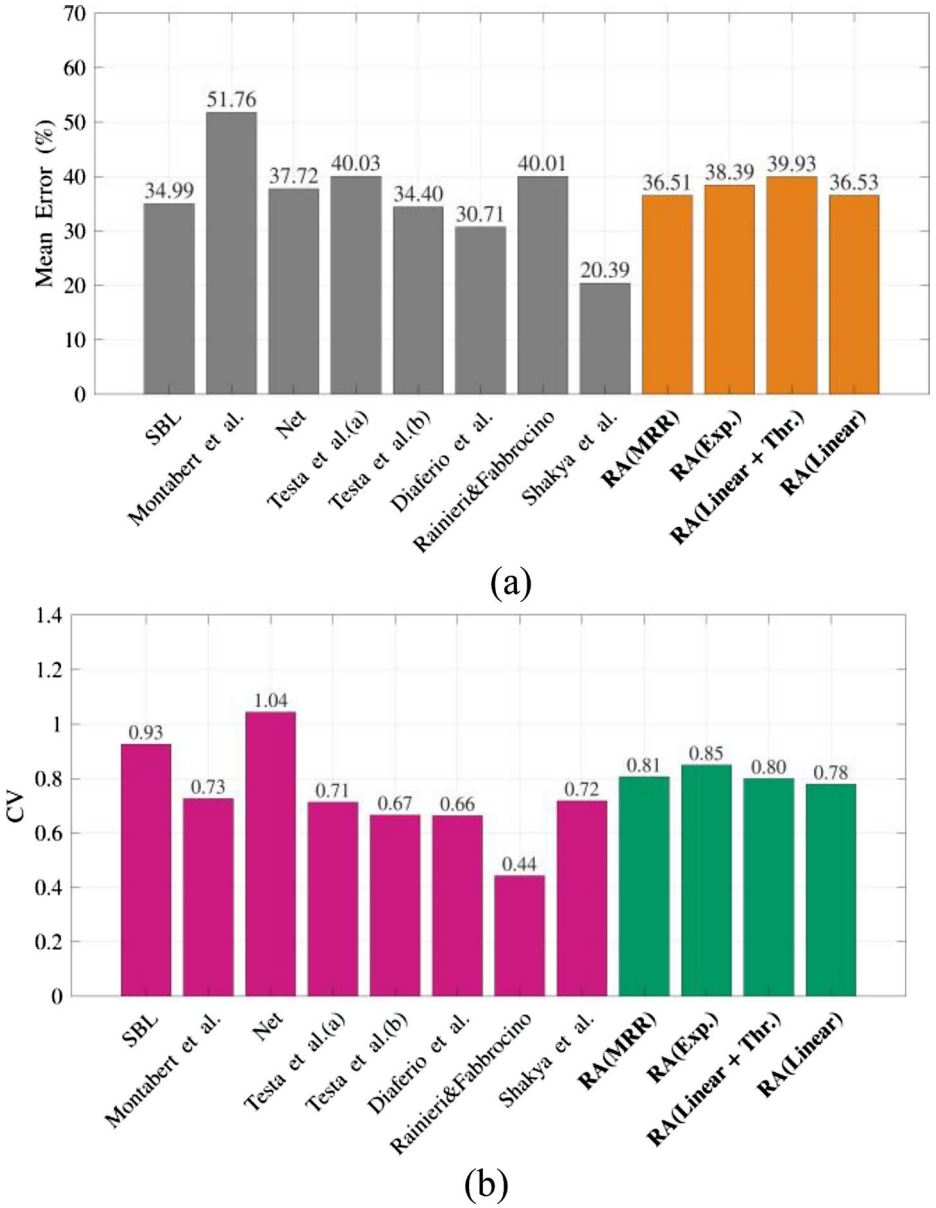

Fig. 15 Validation dataset A (geometric parameters): (**a**) mean prediction error for different candidate models (grey) and different RA weighting strategies (orange); (**b**) coefficient of variation for different candidate models (magenta) and different RA weighting strategies (green)

rapid assessment of the dynamic behavior of masonry towers, capitalizing on the complementary knowledge embedded in the available models. This enhances the generality and robustness of the results, especially when applied to structures with limited or uncertain input data.

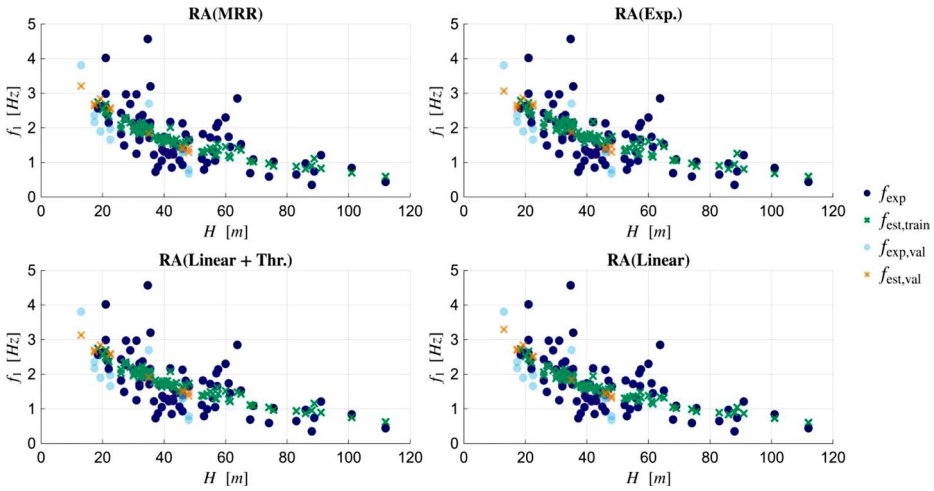

Fig. 16 Dataset A (geometric parameters): experimental vs. predicted frequencies using rank aggregation according to the different proposed weighting strategies (MRR = mean reciprocal ranking, Exp. = exponential decay, Linear + Thr. = linear with a threshold, and Linear). Dark blue circles represent the experimental fundamental frequency for the training dataset, while light blue circles denote those of the validation dataset. Magenta crosses indicate the frequency estimated by the RA techniques for the training data, and grey crosses represent the corresponding estimates for the validation set

- Despite these advantages, the method is subject to intrinsic limitations. The geometric and mechanical variables used as predictors cannot fully capture the complex dynamic behavior of bounded masonry towers, which is influenced by many factors. The errors obtained in this study are consistent with those reported in the literature (Bartoli et al. 2017, 2020), confirming the inherent variability associated with such predictive models. Moreover, while the RA framework provides an effective tool for comparative and interpretative purposes, its direct application by practitioners may be challenging, as it requires computational implementation and access to multiple predictive models. In particular, data-driven methods (i.e., neural networks or SBL models), unlike empirical laws with straightforward formulae, are not readily usable by practitioners, which limits their applicability in rapid assessments. For this reason, the proposed approach is primarily intended as a research and decision-support tool. However, in future developments, a user-friendly public tool with a graphical interface could be implemented to overcome this limitation and enhance the practical usability of the method. Furthermore, lower estimation errors can be achieved through extended experimental campaigns on a larger number of towers over time, which would contribute to expanding the database and reducing current uncertainties.

4 Conclusions

The fundamental frequency estimation of historic masonry towers plays a key role in the structural health monitoring of vulnerable heritage assets. This study presented a rank aggregation strategy for estimating the fundamental frequency of historic bounded masonry

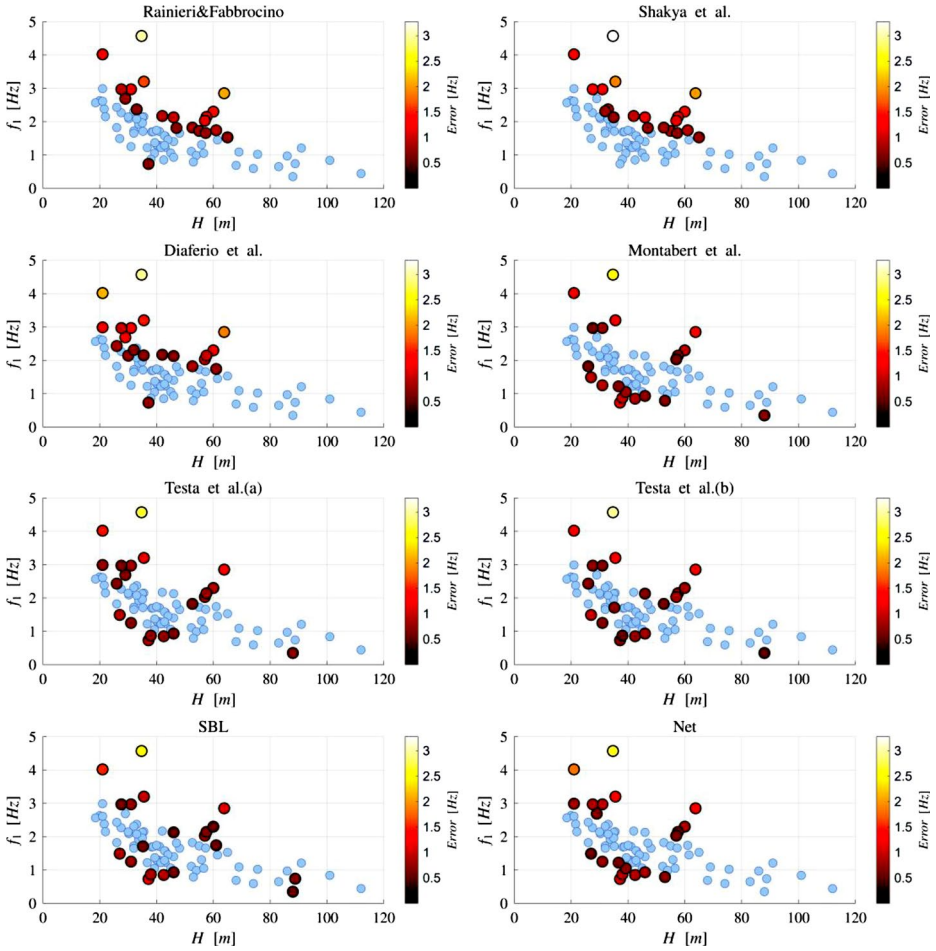

Fig. 17 Dataset A (geometric parameters): outlier analysis on the upper 25% of data with the highest prediction errors (estimation laws). The scatter plots show the comparison between the experimental and aggregated predicted fundamental frequencies of bounded masonry towers as a function of total height (H). Lighter tones (yellow) correspond to higher errors, while darker tones (red to black) denote smaller discrepancies between experimental and predicted values

towers, combining outputs from empirical and data-driven models through a probabilistic framework based on the Plackett-Luce model. The ranking procedure orders the candidates by maximizing the likelihood of their consistency with experimental data, while, at the same time, aiming to reduce variability across the different predictive models. Although each empirical law is individually valid and reliable within its respective domain, they are jointly used to harness their complementary strengths. The rank aggregation method was tested under two distinct scenarios: one using only geometric parameters, and another including both geometric and mechanical properties:

- In the first case, where only geometric information was available, the rank aggregation model, weighted with different strategies, achieved comparable performance to the best

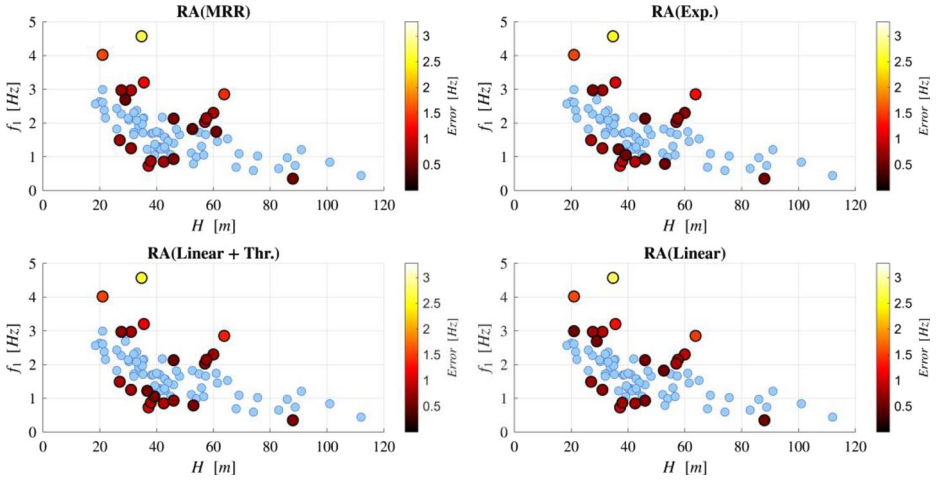

Fig. 18 Dataset A (geometric parameters): outlier analysis on the upper 25% of data with the highest prediction errors (RA). The scatter plots show the comparison between the experimental and aggregated predicted fundamental frequencies of bounded masonry towers as a function of total height (H). Lighter tones (yellow) correspond to higher errors, while darker tones (red to black) denote smaller discrepancies between experimental and predicted values

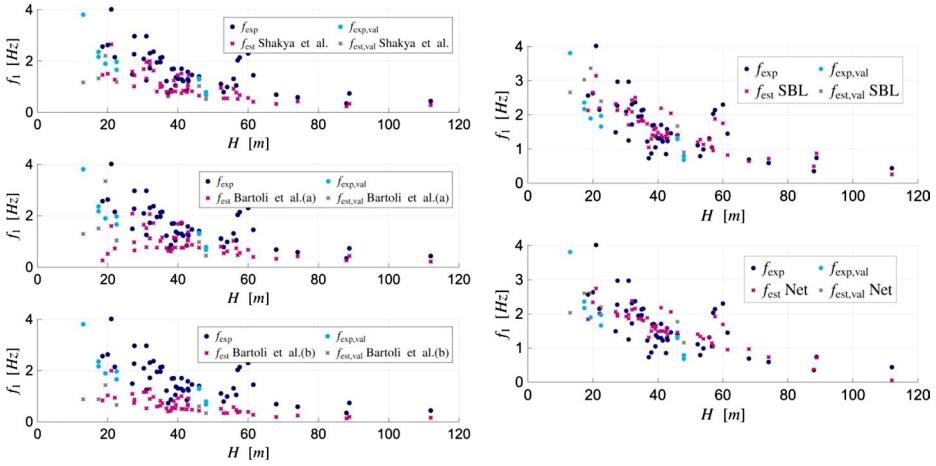

Fig. 19 Dataset B (geometric and mechanical parameters): comparison between estimated and experimental fundamental frequencies of masonry towers as a function of the total height H for each candidate model. Dark blue circles represent the experimental fundamental frequency for the training dataset, while light blue circles denote those of the validation dataset. Magenta crosses indicate the frequency estimated by each candidate for the training data, and grey crosses represent the corresponding estimates for the validation set

ranked selected candidate, particularly in the training phase resulting in a mean error of 26.73%. In the validation phase, the rank aggregation model does not outperform every candidate, resulting in a mean error of 36.51%.

- In the second scenario, including both geometric and mechanical parameters, the rank

Table 12 Dataset B (geometric and mechanical parameters): reference ranking list for candidates based on geometric and mechanical parameters. The number p represents the row of the permutation matrix $\mathbf{C}$ which describes the best ranking

P	1st	2nd	3rd	4th	5th
30	SBL	Net	Shakya et al. (2016)	Bartoli et al. (2017) (a)	Bartoli et al. (2017) (b)

aggregation model consistently outperformed all candidates in both the training and validation phases. In detail, based on the different weighting strategies, it achieved a lower mean prediction error in both the training (20.83%) and validation (14.74%) phases compared to the first ranked individual model, Sparse Bayesian Learning, which exhibited mean errors of 21.13% in the training and 34.57% in the validation phases.

These outcomes also translate into several considerations that support the practical relevance of the rank aggregation strategy.

- The greater performance of the rank aggregation approach in the second scenario can be attributed to the integration of mechanical properties in the predictive framework. In practical terms, the proposed method offers a flexible and reliable tool for the preliminary dynamic assessment of historic masonry towers, especially when both geometric and mechanical data are accessible. The improvement brought by the information on mechanical properties could be associated with the still limited number of empirical laws based on the geometric and mechanical properties of the towers, thus leaving room for improvement.
- The method is flexible and can be updated as new experimental data become available or as additional predictive models are developed, making it a useful strategy for applications in the conservation of heritage structures. In addition, the use of models based on different input parameters broadens the applicability of the approach, proving it to be effective even when only limited information on the structure is available.

It is worth noting that the estimation of the first natural frequency of historic masonry towers remains affected by important uncertainty. This is primarily due to the intrinsic complexity of the problem (e.g., material heterogeneity, boundary conditions, construction history, and limited observability), which limits the ability of an optimal frequency law to accurately predict the response of towers. Moreover, increasing the number of variables does not necessarily improve predictive performance, sometimes making formulations based on the tower total and effective height more effective, which, according to the literature, remain the most important variables to consider.

Future developments will target improving the ranking procedure, for instance by refining the weighting criteria assigned to each candidate model, or by including uncertainty within the prediction process. Moreover, broadening the reference dataset to include a more diverse range of structural configurations and boundary conditions would contribute to further validating the method. In addition, it will be beneficial to tailor the rank aggregation framework to groups of towers with similar properties; for these subsets, rank aggregation may lead to even better results. Lastly, future work will also focus on predicting the fundamental frequency of isolated masonry towers, by integrating and aiming at the selection of the models to be considered as candidates within the Plackett-Luce model framework.

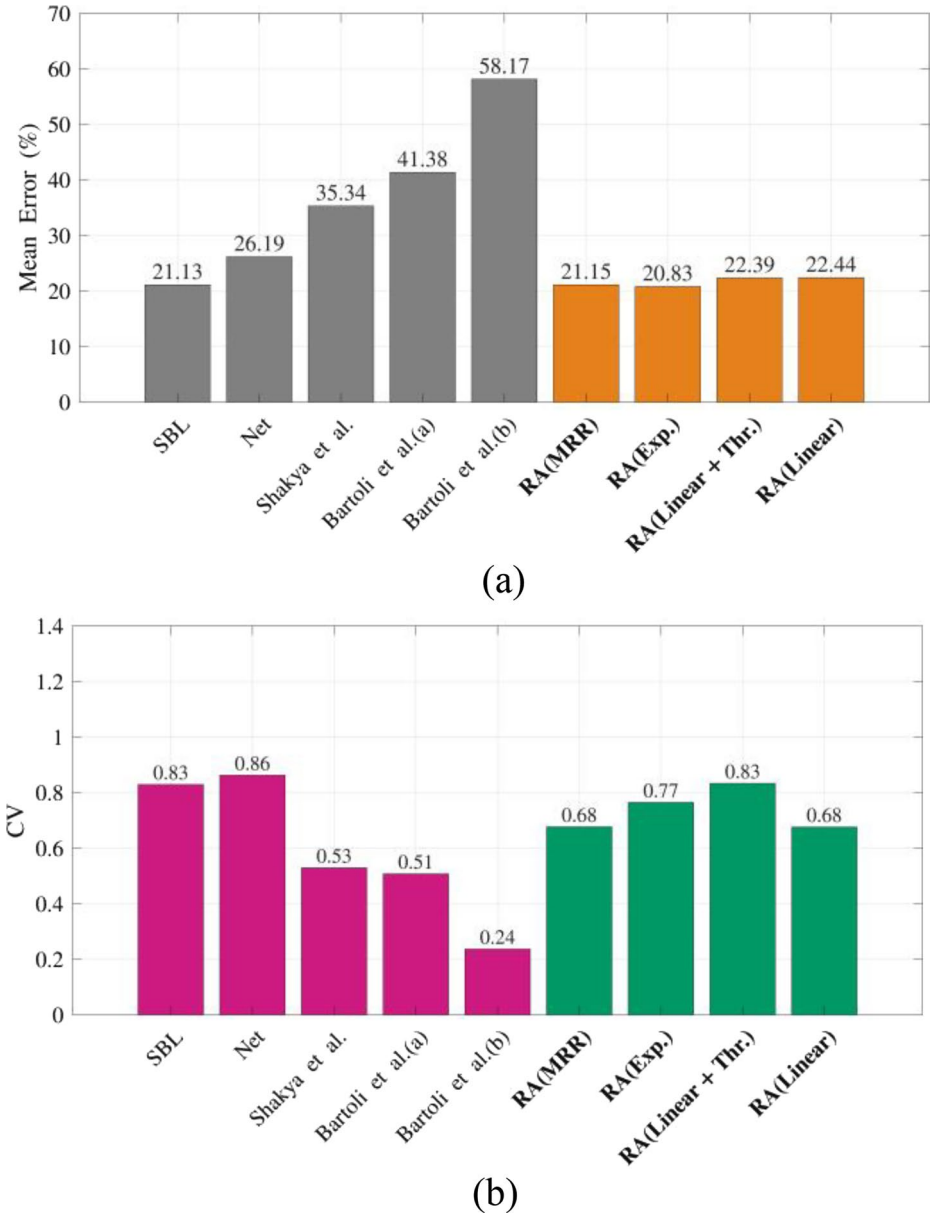

Fig. 20 Training dataset B (geometric and mechanical parameters): (**a**) mean prediction error for different candidate models (grey) and different RA weighting strategies (orange); (**b**) coefficient of variation for different candidate models (magenta) and different RA weighting strategies (green)

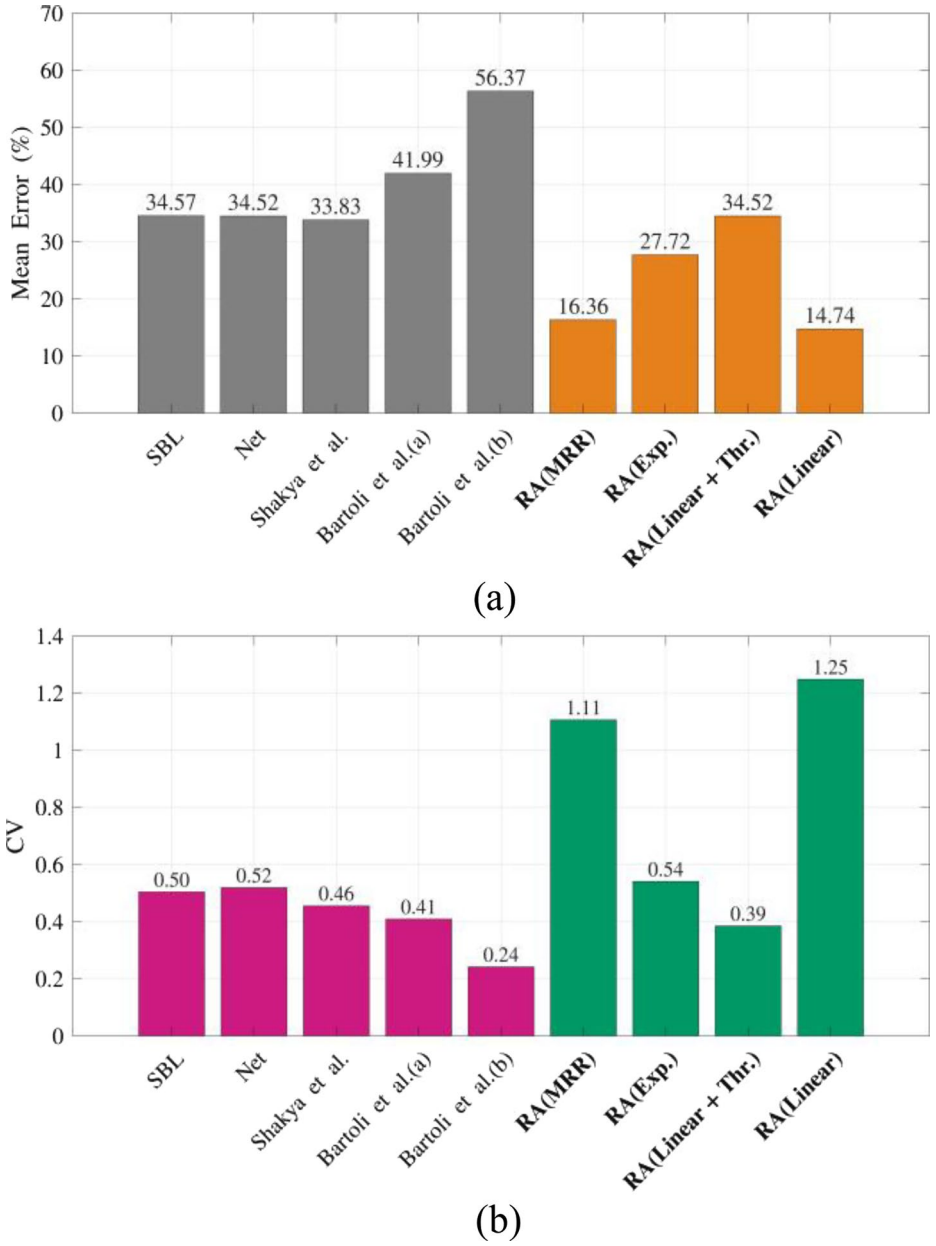

Fig. 21 Validation dataset B (geometric and mechanical parameters): (**a**) mean prediction error for different candidate models (grey) and different RA weighting strategies (orange); (**b**) coefficient of variation for different candidate models (magenta) and different RA weighting strategies (green)

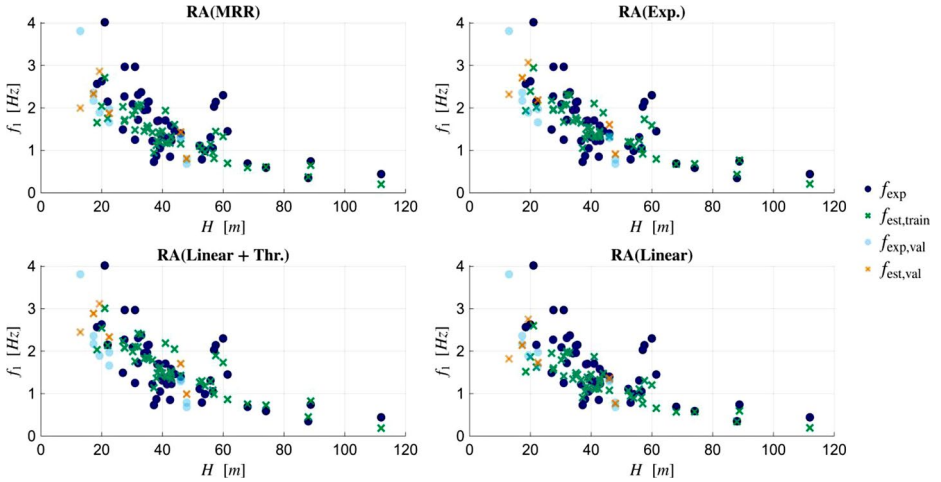

Fig. 22 Dataset B (geometric and mechanical parameters): experimental vs. predicted frequencies using rank aggregation according to the different proposed weighting strategies (MRR = mean reciprocal ranking, Exp. = exponential decay, Linear + Thr. = linear with a threshold, and Linear). Dark blue circles represent the experimental fundamental frequency for the training dataset, while light blue circles denote those of the validation dataset. Magenta crosses indicate the frequency estimated by the RA techniques for the training data, and grey crosses represent the corresponding estimates for the validation set

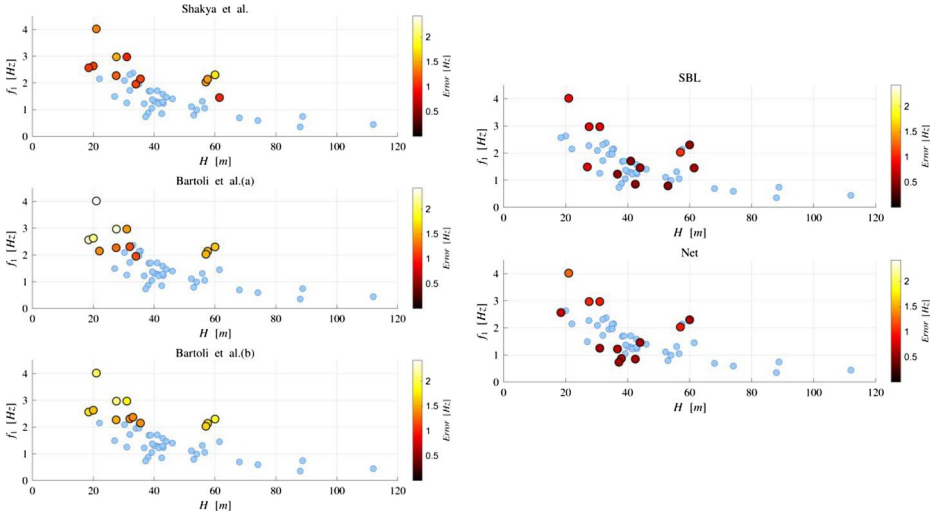

Fig. 23 Dataset B (geometric and mechanical parameters): outlier analysis on the upper 25% of data with the highest prediction errors (estimation laws). The scatter plots show the comparison between the experimental and aggregated predicted fundamental frequencies of bounded masonry towers as a function of total height (H). Lighter tones (yellow) correspond to higher errors, while darker tones (red to black) denote smaller discrepancies between experimental and predicted values

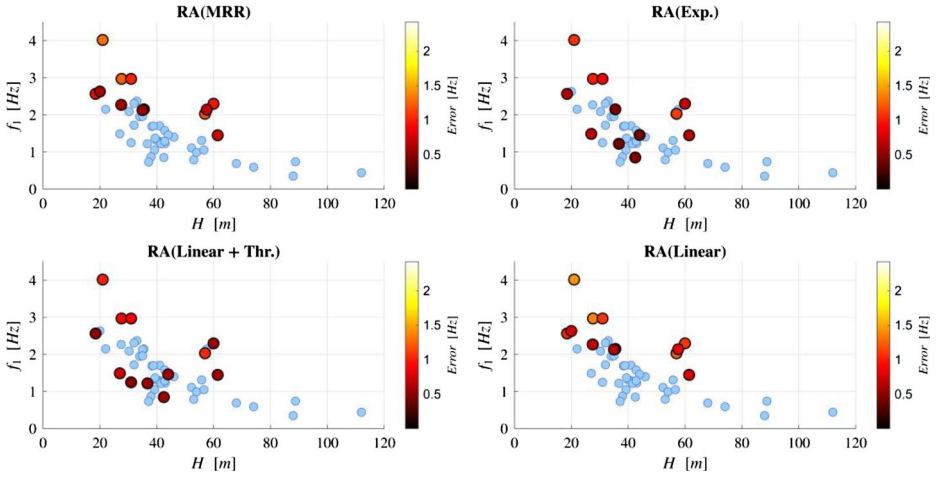

Fig. 24 Dataset B (geometric and mechanical parameters): outlier analysis on the upper 25% of data with the highest prediction errors (RA). The scatter plots show the comparison between the experimental and aggregated predicted fundamental frequencies of bounded masonry towers as a function of total height (H). Lighter tones (yellow) correspond to higher errors, while darker tones (red to black) denote smaller discrepancies between experimental and predicted values

Acknowledgements This publication is part of the project PNRR-NGEU which has received funding from the MUR – DM 118/2023. This study was carried out within the «SAT4SHM» project—funded by European Union—Next Generation EU within the PRIN 2022 PNRR program (D.D.1409, 14/09/2022 MIUR).

Author contributions Conceptualization A.C., R.C. and G.M.; Methodology A.C. and G.M.; Validation A.C. and G.M.; Formal analysis A.C. and G.M.; Investigation A.C., G.M. and R.C.; Resources A.C. and G.M.; Data curation A.C. and G.M.; Writing—original draft preparation A.C.; Writing—review and editing A.C., G.M. and R.C.; Visualization A.C., G.M. and R.C.; Supervision R.C. and G.M.; Project administration, R.C.; Funding acquisition, R.C.

Funding Open access funding provided by Politecnico di Torino within the CRUI-CARE Agreement. This work was supported by: project PNRR-NGEU which has received funding from the MUR – DM 118/2023. Next Generation EU within the PRIN 2022 PNRR program, Grant/Award. Number: D.D.1409, 14/09/2022 MIUR.

Data availability Data employed in the current study are available from the corresponding author on reasonable request.

Declarations

Competing interests The authors declare that they have no known competing financial interests or personal relationships that could have appeared to influence the work reported in this paper.

References

Azzara R, Girardi M, Padovani C, Pellegrini D (2019) Experimental and numerical investigations on the seismic behaviour of the San Frediano bell tower in Lucca. Ann Geophys 61. https://doi.org/10.4401/ag-8025

Bama SS, Ahmed MI, Saravanan A (2015) A survey on performance evaluation measures for information retrieval system. Int J Res Eng Technol 2(2):1015–1020

Bartoli G, Betti M, Giordano S (2013) In situ static and dynamic investigations on the "Torre Grossa" masonry tower. Eng Struct 52:718–733. https://doi.org/10.1016/j.engstruct.2013.01.030

Bartoli G, Betti M, Marra AM, Monchetti S (2020) On the role played by the openings on the first frequency of historic masonry towers. Bull Earthq Eng 18(2):427–451. https://doi.org/10.1007/s10518-019-00662-9

Bartoli G, Betti M, Marra Antonino M, Monchetti S (2017) Semiempirical formulations for estimating the Main frequency of slender masonry towers. J Perform Constr Facil 31(4):04017025. https://doi.org/10.1061/(ASCE)CF.1943-5509.0001017

Bartoli G, Betti M, Vignoli A (2016) A numerical study on seismic risk assessment of historic masonry towers: a case study in San Gimignano. Bull Earthq Eng 14(6):1475–1518. https://doi.org/10.1007/s10518-016-9892-9

Bassoli E, Vincenzi L, D'Altri AM, de Miranda S, Forghieri M, Castellazzi G (2018) Ambient vibration-based finite element model updating of an earthquake-damaged masonry tower. Struct Control Health Monit 25(5):e2150. https://doi.org/10.1002/stc.2150

Bayraktar A, Çalik İ, Türker T (2022) A simplified fundamental frequency formulation based on in-situ Tests for masonry stone minarets. Exp Tech 46(2):225–238. https://doi.org/10.1007/s40799-021-00474-0

Beconcini ML, Croce P (2006) Dynamic monitoring and model updating of a masonry bell tower in Pisa. In Proc. 5th Int. Conf. on Structural Analysis of Historical Constructions

Bianconi F, Salachoris GP, Clementi F, Lenci S (2020) A genetic algorithm procedure for the automatic updating of FEM based on Ambient Vibration Tests. Sensors 20(11):3315. https://doi.org/10.3390/s20113315

Binda L, Falco M, Poggi M, Zasso C, Mirabella Roberti A, Corradi G, R, Tongini R (2000) Static and dynamic studies on the Torrazzo in Cremona (Italy): the highest masorny bell tower in Europe

Bonato P, Ceravolo R, De Stefano A, Molinari F (2000). Cross-time-frequency techniques for the identification of masonry buildings. Mech Syst Signal Process. 14(1):91–109

Bongiovanni G, Clemente P, Buffarini G (2000) Analysis of the seismic response of a damaged masonry bell tower

Bru D, Ivorra S, Betti M, Adam JM, Bartoli G (2019) Parametric dynamic interaction assessment between bells and supporting slender masonry tower. Mech Syst Signal Process 129:235–249. https://doi.org/10.1016/j.ymssp.2019.04.038

Cabboi A, Gentile C, Saisi A (2017) From continuous vibration monitoring to FEM-based damage assessment: application on a stone-masonry tower. Constr Build Mater 156:252–265. https://doi.org/10.1016/j.conbuildmat.2017.08.160

Çalik İ, Bayraktar A, Türker T, Akköse M (2020) Empirical formulation for estimating the fundamental frequency of historical stone mosques with masonry domes. Struct Des Tall Spec Build 29(9). https://doi.org/10.1002/tal.1732

Cao Z, Qin T, Liu T-Y, Tsai M-F, Li H (2007) Learning to rank. In Proceedings of the 24th International Conference on Machine Learning, pp 129–136). https://doi.org/10.1145/1273496.1273513

Capanna I, Cirella R, Aloisio A, Alaggio R, Di Fabio F, Fragiacomo M (2021) Operational modal analysis, model update and fragility curves estimation, through truncated incremental dynamic analysis, of a masonry Belfry. Buildings 11(3):120. https://doi.org/10.3390/buildings11030120

Carone AS, Foti D, Giannoccaro NI, Nobile R (2013) Non-destructive characterization and dynamic identification of an historical bell tower. In 4th International Conference on Integrity, Reliability and Failure of Mechanical Systems. IRF'13, *Funchal/Madeira*

Casarin F, Modena C, Simonato E (2009) Dynamic identification of the St. Martin bell-tower of Burano, Venice. In IOMAC, 2009 - 3rd International Operational Modal Analysis Conference, (pp 475–482). https://www.scopus.com/inward/record.uri?eid=2-s2.0-84906240477%26;partnerID=40%26;md5=6d0357b87268d27c10a6e385c1c0fa99

Casciati S, Al-Saleh R (2010) Dynamic behavior of a masonry civic belfry under operational conditions. Acta Mech 215(1):211–224. https://doi.org/10.1007/s00707-010-0343-4

Cavaleri L, Ferrotto M, Di Trapani F, Vicentini A (2019) Vibration Tests and structural identification of the Bell tower of Palermo Cathedral. Open Construct Build Technol J 13:319–330. https://doi.org/10.2174/1874836801913010319

Ceravolo R, Matta E, Quattrone A, Zanotti Fragonara L (2017) Amplitude dependence of equivalent modal parameters in monitored buildings during earthquake swarms. Earthq Eng Struct Dyn 46(14):2399–2417. https://doi.org/10.1002/eqe.2910

Ceravolo R, Pistone G, Fragonara LZ, Massetto S, Abbiati G (2016) Vibration-based monitoring and diagnosis of Cultural Heritage: a methodological discussion in three examples. IJAH 10(4):375–395. https://doi.org/10.1080/15583058.2013.850554

Ceriotti M, Mottola L, Picco G, Murphy A, Guna S, Corrà M, Pozzi M, Zonta D, Zanon P (2009) Monitoring heritage buildings with wireless sensor networks. The Torre Aquila Deployment. https://doi.org/10.1145/1602165.1602191

Ceroni F, Marisa P, Simona V, Manfredi G (2009) Historical, architectural, and structural assessment of the bell tower of Santa Maria del Carmine. IJAH 3(3):169–194. https://doi.org/10.1080/15583050802347490

Clementi F, Pierdicca A, Formisano A, Catinari F, Lenci S (2017) Numerical model upgrading of a historical masonry building damaged during the 2016 Italian earthquakes: the case study of the Podestà palace in Montelupone (Italy). J Civ Struct Health Monit 7(5):703–717. https://doi.org/10.1007/s13349-017-0253-4

Colapietro D, Fiore A, Netti A, Fatiguso F, Marano G, Fino M, D C, A A (2013) Dynamic identification and evaluation of the seismic safety of a masonry bell tower in the south of Italy. https://doi.org/10.7712/120113.4751.C1418

Coletta G, Miraglia G, Ceravolo R, Surace C (2020) Ensemble technique for Machine learning with application to monitoring of Heritage structures. In Wahab MA (ed) Proceedings of the 13th International Conference on Damage Assessment of Structures, Springer Singapore (pp. 333–349)

Cosenza E, Iervolino I (2007) Case study: seismic retrofitting of a medieval Bell tower with FRP. J Compos Constr 11(3):319–327. https://doi.org/10.1061/(ASCE)1090-0268(2007)11:3(319)

Cunha Á, Ramos LF, Magalhães F, Lourenço PB (2014) Dynamic identification and modelling of Clérigos Tower: initial studies

De Stefano A, Ceravolo R (2007) Assessing the Health state of Ancient structures: the role of vibrational Tests. J Intell Mater Syst Struct 18:793–807. https://doi.org/10.1177/1045389X06074610

Diaferio M, Foti D, Giannoccaro NI (2014) Non-destructive characterization and identification of the modal parameters of an old masonry tower. In 2014 IEEE Workshop on Environmental, Energy, and Structural Monitoring Systems Proceedings, (pp 1–6). https://doi.org/10.1109/EESMS.2014.6923265

Diaferio, M., Foti, D., Giannoccaro, N. I., Ivorra, S. (2019). Health monitoring through a tuned Fe model of a medieval tower placed in a landslide area. In: Proceedings of the 5th International Conference on Mechanical Models in Structural Engineering (CMMoST 2019); 2019 Oct 23–25; San Vicente (Alicante), Spain. Alicante: Editorial Club Universitario. p. 379–394. ISBN: 978–84–17924–58–4

Diaferio M, Foti D, Giannoccaro NI, Ivorra S (2017) Model updating based on the dynamic identification of a baroque bell tower. Int J Saf Secur Eng 7:519–531. https://doi.org/10.2495/SAFE-V7-N4-519-531

Diaferio M, Foti D, Potenza F (2018) Prediction of the fundamental frequencies and modal shapes of historic masonry towers by empirical equations based on experimental data. Eng Struct 156:433–442. https://doi.org/10.1016/j.engstruct.2017.11.061

DPCM (2011) Direttiva del Presidente del Consiglio dei Ministri per la valutazione e riduzione del rischio sismico del patrimonio culturale con riferimento alle norme tecniche per le costruzioni di cui al decreto del Ministero delle infrastrutture e dei trasporti de. G.U. Feb 26;No. 47. (In Italian)

Faccio P, Podestà S, Saetta A (2010) Venezia, Campanile della Chiesa di Sant'Antonio, Esempi Applicativi - D. in: Linee Guida per la valutazione e riduzione del rischio sismico del patrimonio culturale allineate alle nuove Norme tecniche per le costruzioni (d.m. 14 gennaio 2008), (In Italian)

Farrar CR, Worden K (2006, (1851) An introduction to structural health monitoring. Philos Trans A Math Phys Eng Sci 365(1851):303–315. https://doi.org/10.1098/rsta.2006.1928

Ferraioli M, Miccoli L, Abruzzese D (2018) Dynamic characterisation of a historic bell-tower using a sensitivity-based technique for model tuning. J Civ Struct Health Monit 8:253–269. https://doi.org/10.1007/s13349-018-0272-9

Foti D, Diaferio M, Giannoccaro NI, Mongelli M (2012) Ambient vibration testing, dynamic identification and model updating of a historic tower. NDT E Inter 47:88–95. https://doi.org/10.1016/j.ndteint.2011.11.009

Foti D, Ivorra S, Sabbà M (2012) Dynamic investigation of an Ancient masonry Bell tower with operational modal analysis - a Non-destructive experimental technique to obtain the dynamic characteristics of a structure. Open Construct Build Technol J 6:384–391. https://doi.org/10.2174/1874836801206010384

Fuentes R, Dervilis N, Worden K, Cross EJ (2019) Efficient parameter identification and model selection in nonlinear dynamical systems via sparse Bayesian learning. J Phys Conf Ser 1264(1):012050. https://doi.org/10.1088/1742-6596/1264/1/012050

Furlan M (2015) Monitoraggio dinamico e modellazione strutturale per la valutazione del comportamento sismico di Castelvecchio, Verona. MSc Thesis

Gentile C, Ruccolo A, Saisi A (2019) Long-term Vibration measurements to enhance the knowledge of a historic Bell-tower. In: Aguilar R, Torrealva D, Moreira S, Pando MA, Ramos LF (eds) Structural analysis of historical constructions. Springer International Publishing, pp 2236–2244

Gentile C, Saisi A (2007) Ambient vibration testing of historic masonry towers for structural identification and damage assessment. Constr Build Mater 21(6):1311–1321. https://doi.org/10.1016/j.conbuildmat.2006.01.007

Gentile C, Saisi A, Borlenghi P (2019) FE modelling for seismic assessment of an Ancient tower from Ambient Vibration survey

Goodfellow I, Bengio Y, Courville A (2016) Deep learning. MIT press

Guiver J, Snelson E (2009) Bayesian inference for Plackett-Luce ranking models. In Proceedings of the 26th Annual International Conference on Machine Learning, pp (377–384). https://doi.org/10.1145/1553374.1553423

Ivorra S, Cervera JR (2002) Analysis of the dynamic actions when bells are swinging on the bell-tower of Bonrepos i Mirambell Church (Valencia, Spain). In Proceedings of the 2002 International Conference on Noise and Vibration Engineering, ISMA, pp 2343–2348

Ivorra S, Pallarés F, Adam J (2009) Experimental and numerical results from the seismic study of a masonry Bell tower. Adv Struct Eng 12:287–293. https://doi.org/10.1260/136943309788251641

Ivorra S, Pallarés FJ (2006) Dynamic investigations on a masonry bell tower. Eng Struct 28(5):660–667. https://doi.org/10.1016/j.engstruct.2005.09.019

Ivorra S, Pallarés FJ, Adam JM, Tomás R (2010) An evaluation of the incidence of soil subsidence on the dynamic behaviour of a gothic bell tower. Eng Struct 32(8):2318–2325. https://doi.org/10.1016/j.engstruct.2010.04.007

Jardim CM, Mendes LA, Gonçalve AM (2013) Dynamic characterization of the Funchal's cathedral bell tower. In Proceedings of the 5th International Operational Modal Analysis Conference, *May*, Guimaraes, Portugal, 13–15

Júlio ENBS, da Silva Rebelo CA, Dias-da-Costa DASG (2008) Structural assessment of the tower of the University of Coimbra by modal identification. Eng Struct 30(12):3468–3477. https://doi.org/10.1016/j.engstruct.2008.06.001

Lopez S, D'Amato M, Ramos L, Laterza M, Lourenço PB (2019) Simplified formulations for estimating the Main frequencies of Ancient masonry churches. Front Built Environ 5. https://doi.org/10.3389/fbuil.2019.00018

Luce RD (1959) Individual choice behavior. *John Wiley*

Manikandan K, Nidhi M, Micelli F, Cascardi A, Sivasubramanian MVR (2024) Fundamental frequency formulation and modeling of masonry slender structures: a comparative study of machine learning and regression techniques. Eng Fail Anal 162:108420. https://doi.org/10.1016/j.engfailanal.2024.108420

The MathWorks Inc (2022) Natick, Massachusetts: the MathWorks Inc., MATLAB version: 9.13.0 https://www.Mathworks.Com

Milani G, Casolo S, Naliato A, Tralli A (2012) Seismic assessment of a medieval masonry tower in Northern Italy by limit, nonlinear Static, and full dynamic analyses. IJAH 6(5):489–524. https://doi.org/10.1080/15583058.2011.588987

Minsky M, Papert SA (2017) Perceptrons: an introduction to computational geometry. The MIT Press. https://doi.org/10.7551/mitpress/11301.001.0001

Miraglia G, Lenticchia E, Ceravolo R, Betti R (2019) Synergistic and combinatorial optimization of finite element models for monitored buildings. Struct Control Health Monit 26(9):e2403. https://doi.org/10.1002/stc.2403

Montabert A, Giry C, Schraen C, Lépine J, Choueiri C, Mercerat ED, Gueguen P (2023) An open database to evaluate the fundamental frequency of historical masonry towers through empirical and physics-based formulations. Buildings 13:2168. https://doi.org/10.3390/buildings13092168

Montabert A, Mercerat ED, Clément J, Langlaude P, Lyon-Caen H, Lancieri M (2022) High resolution operational modal analysis of Sant'Agata del Mugello in light of its building history. Eng Struct 254:113767. https://doi.org/10.1016/j.engstruct.2021.113767

Nochebuena-Mora E, Mendes N, Lourenço PB, Greco F (2021) Dynamic behavior of a masonry bell tower subjected to actions caused by bell swinging. Structures 34:1798–1810. https://doi.org/10.1016/j.istruc.2021.08.066

Oliveira CS, Çaktı E, Stengel D, Branco M (2012) Minaret behavior under earthquake loading: the case of historical Istanbul. Earthq Eng Struct Dyn 41(1):19–39. https://doi.org/10.1002/eqe.1115

Oliveira CS, Eser Ç, Vitor C, Dar E (2023) Revisiting the frequency laws for Ottoman minarets. Analysis of uncertainties. IJAH 17(10):1648–1668. https://doi.org/10.1080/15583058.2022.2057881

Pavlovic M, Trevisani S, Cecchi A (2019) A procedure for the structural identification of masonry towers. J Nondestruct Eval 38. https://doi.org/10.1007/s10921-019-0575-8

Peeters B, Sforza G, Sbaraglia L, Germano F (2011) Efficient operational modal testing and analysis for design verification and restoration baseline assessment: Italian case studies. In Proceedings of the Experimental Vibration Analysis for Civil Engineering Structures (EVACES), pp 3–5

Pieraccini M, Dei D, Betti M, Bartoli G, Tucci G, Guardini N (2014) Dynamic identification of historic masonry towers through an expeditious and no-contact approach: application to the "Torre del Mangia" in Siena (Italy). J Cult Herit 15(3):275–282. https://doi.org/10.1016/j.culher.2013.07.006

Plackett RL (1975) The analysis of permutations. J R Stat Soc Ser C Appl Stat 24(2):193–202. https://doi.org/10.2307/2346567

Rainieri C, Fabbrocino G (2011) Predictive correlations for the estimation of the elastic period of masonry towers

Ramos LF, Aguilar R, Lourenço PB, Moreira S (2013) Dynamic structural health monitoring of Saint Torcato church. Mech Syst Signal Process 35(1–2):1–15. https://doi.org/10.1016/j.ymssp.2012.09.007

Ramos LF, Marques L, Lourenço PB, De Roeck G, Campos-Costa A, Roque J (2010) Monitoring historical masonry structures with operational modal analysis: two case studies. Mech Syst Signal Process 24(5):1291–1305. https://doi.org/10.1016/j.ymssp.2010.01.011

Ranstam J, Cook JA (2018) LASSO regression. Br J Surg 105(10):1348

Sabia D, Aoki T, Cosentini R, Lancellotta R (2015) Model updating to forecast the dynamic behavior of the Ghirlandina Tower in Modena, Italy. J Earthq Eng 19. https://doi.org/10.1080/13632469.2014.962668

Saisi A, Gentile C, Guidobaldi M (2015) Post-earthquake continuous dynamic monitoring of the Gabbia Tower in Mantua, Italy. Constr Build Mater 81:101–112. https://doi.org/10.1016/j.conbuildmat.2015.02.010

Saloustros S, Pelà L, Roca P (2020) Nonlinear numerical modeling of complex masonry Heritage structures considering history-related phenomena in staged Construction analysis and material uncertainty in seismic assessment. J Perform Constr Facil 34(5):04020096. https://doi.org/10.1061/(ASCE)CF.1943-5509.0001494

Schmidt T (2007) Dynamic behavior of twin bell towers

Scussolini L, Foti V, Civera M, Ceravolo R, Pistone G (2023) Redesign of strengthening interventions on historical buildings. The case study of an earthquake-damaged Bell tower. In: Limongelli MP, Giordano PF, Quqa S, Gentile C, Cigada A (eds) Experimental vibration analysis for civil engineering structures. Springer Nature Switzerland, pp 708–717. https://doi.org/10.1007/978-3-031-39109-5_72

Serhatoğlu C, Livaoğlu R (2019) A fast and practical approximations for fundamental period of historical Ottoman minarets. Soil Dyn Earthq Eng 120:320–331. https://doi.org/10.1016/j.soildyn.2019.02.010

Shakya M, Varum H, Vicente R, Costa A (2016) Empirical formulation for estimating the fundamental frequency of slender masonry structures. IJAH 10(1):55–66. https://doi.org/10.1080/15583058.2014.951796

Sorrentino L, Doria M, Tassi V, Liotta M (2019) Performance of a Far-field historical Church during the 2016–2017 central Italy earthquakes. J Perform Constr Facil. https://doi.org/10.1061/(ASCE)CF.1943-5509.0001273

Standoli G, Salachoris GP, Masciotta M, Clementi F (2021) Combining operational modal analysis and genetic algorithms to understand the actual structural behavior of historical constructions. https://doi.org/10.7712/120121.8501.19333

Testa F, Barontini A, Lourenco P (2023) Database historic masonry towers experimental frequency. Mendeley Data V1. https://doi.org/10.17632/czg2gypj89.1.10.17632/czg2gypj89.1

Testa F, Barontini A, Lourenço PB (2024) Development and validation of empirical formulations for predicting the frequency of historic masonry towers. IJAH 18(7):1164–1184. https://doi.org/10.1080/15583058.2023.2217127

Tipping M (2001) Sparse Bayesian learning and Relevance vector Machine. J Mach Learn Res 1:211–244. https://doi.org/10.1162/15324430152748236

Ubertini F, Comanducci G, Cavalagli N, Laura Pisello A, Luigi Materazzi A, Cotana F (2017) Environmental effects on natural frequencies of the San Pietro bell tower in Perugia, Italy, and their removal for structural performance assessment. Mech Syst Signal Process 82:307–322. https://doi.org/10.1016/j.ymssp.2016.05.025

Venanzi I, Kita A, Cavalagli N, Ierimonti L, Ubertini F (2020) Earthquake-induced damage localization in an historic masonry tower through long-term dynamic monitoring and FE model calibration. Bull Earthq Eng 18(5):2247–2274. https://doi.org/10.1007/s10518-019-00780-4

Yasutake S, Hatano K, Takimoto E, Takeda M (2012) Online rank aggregation. In Asian Conference on Machine Learning, pp 539–553

Zanotti Fragonara L, Boscato G, Ceravolo R, Russo S, Ientile S, Pecorelli ML, Quattrone A (2017) Dynamic investigation on the Mirandola bell tower in post-earthquake scenarios. Bull Earthq Eng 15(1):313–337. https://doi.org/10.1007/s10518-016-9970-z

Zini G, Betti M, Bartoli G, Chiostrini S (2018) Frequency vs time domain identification of heritage structures. Proc Struct Integr 11:460–469. https://doi.org/10.1016/j.prostr.2018.11.115